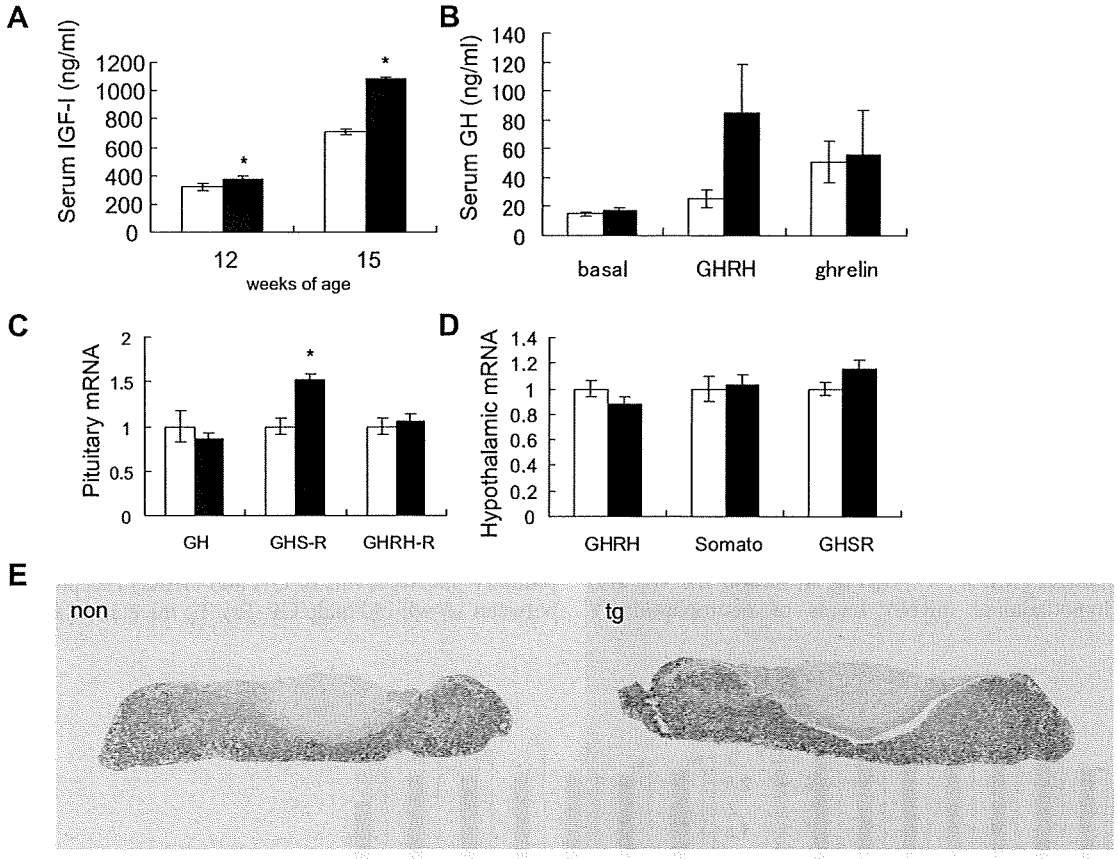

Fig. 5. GH-IGF-I axis in GP-Tag Tg mice. *A*: serum IGF-I levels in male GP-Tag Tg mice (black bars) and nontransgenic littermates (open bars); $n = 7–8$. *B*: serum GH levels at basal state and at 15 min after subcutaneous injection of GH-releasing hormone (GHRH) or ghrelin in male GP-Tag Tg mice (black bars) and nontransgenic littermates (open bars); $n = 8–13$. *C*: pituitary mRNA levels of GH, GHS-R, and GHRH-R in 15-wk-old male GP-Tag Tg mice (black bars) and nontransgenic littermates (open bars); $n = 7$. *D*: hypothalamic mRNA levels of GHRH, somatostatin (somato), and GHS-R in 15-wk-old male GP-Tag Tg mice (black bars) and nontransgenic littermates (open bars); $n = 7$. *E*: pituitary sections of 15-wk-old male Tg mice and non littermates immunostained with anti-GH antibody. $^*P < 0.05$ compared with non littermates.

(NS, $n = 7$; Fig. 5, *C* and *D*). Although plasma ghrelin level was elevated, pituitary GHS-R mRNA level was upregulated in GP-Tag Tg mice ($P < 0.05$, $n = 7$; Fig. 5*C*). We also examined pituitaries of 15-wk-old male GP-Tag Tg mice by immunohistochemical analysis. There were no obvious differences in somatotroph cell number or staining intensity of GH between GP-Tag Tg mice and nontransgenic littermates (Fig. 5*E*).

Glucose metabolism in GP-Tag Tg mice. Blood glucose levels of 15-wk-old male GP-Tag Tg mice were significantly higher than controls ($P < 0.05$, $n = 10$; Fig. 6*A*), although those of 9-wk-old male GP-Tag Tg mice were comparable with the controls (non-Tg vs. Tg: 96.0 ± 4.7 vs. 100.6 ± 4.7, $P = 0.51$, $n = 9$). Intraperitoneal glucose tolerance tests showed significantly higher blood glucose levels in 15-wk-old male GP-Tag Tg mice ($P < 0.05$, $n = 6–11$; Fig. 6*B*). To estimate the insulin sensitivity of GP-Tag Tg mice, we performed an insulin tolerance test. The blood glucose levels after insulin injection in 15-wk-old male GP-Tag Tg mice were suppressed to the same level of those in controls (NS, $n = 5–8$; Fig. 6*C*). Although basal insulin levels of 15-wk-old male GP-Tag Tg mice were not significantly different from those of control mice, those after glucose injection were significantly suppressed in GP-Tag Tg mice ($P < 0.05$, $n = 7–8$; Fig. 6*D*). Pancreatic mRNA and protein levels of insulin in GP-Tag Tg were comparable with those of nontransgenic littermates (NS, $n = 6–8$; Fig. 6, *E* and *F*).

DISCUSSION

In this study, we successfully established a mouse model of ghrelinoma, GP-Tag Tg mouse. GP-Tag Tg mice exhibited chronic elevation of circulating ghrelin with physiological regulation. The elevation of circulating ghrelin in GP-Tag Tg mice (~10-fold elevation) was much higher than that in bacterial artificial chromosome transgenic mice created by Bewick et al. (5) (only ~1.5-fold elevation). Nevertheless, the levels of circulating ghrelin in GP-Tag Tg mice can be considered to be within the physiological range since the highest level of plasma ghrelin observed in the anorexia patients is about seven times higher than those of normal controls (3). One may be confused by low ghrelin mRNA levels and low ghrelin production per milligram of tissue in the stomachs of GP-Tag Tg mice. In general, when the cell cycle progresses, endocrine cell produces far less amounts of hormone since the hormone production occurs mainly at the G_0/G_1 phase of the cell cycle. Since the hyperproliferaing ghrelin-producing cells in GP-Tag Tg mice were forced to proliferate by SV40 T-antigen, which suppresses RB protein and p53, promoting cell cycle progres-

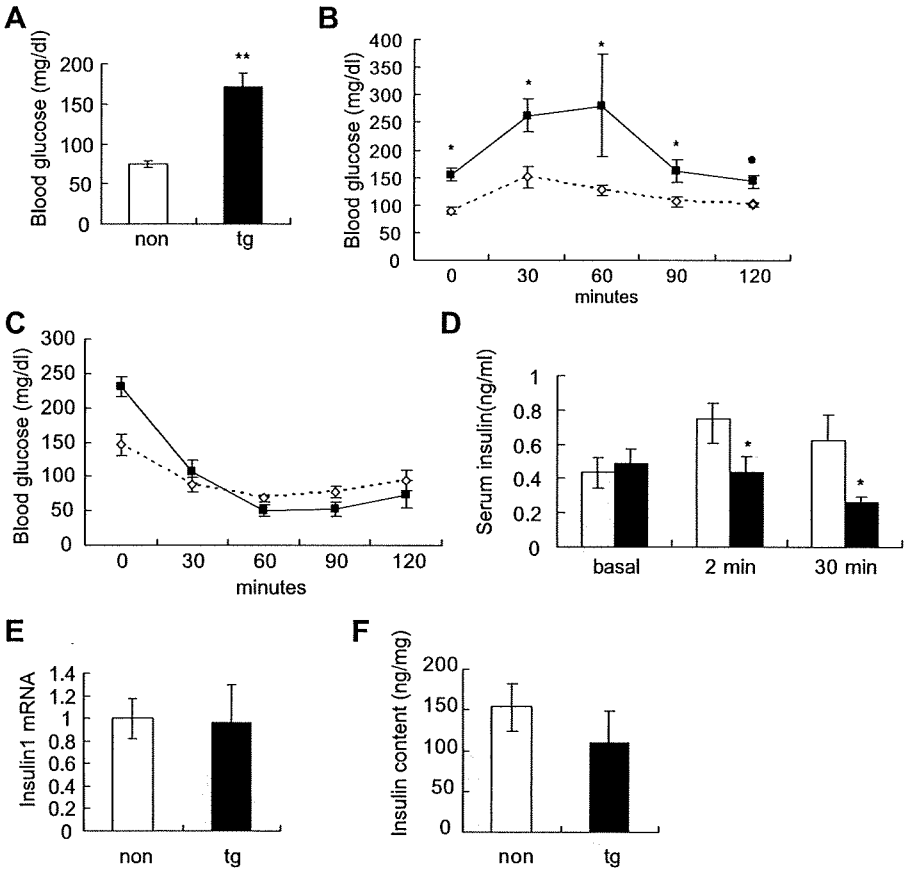

Fig. 6. Glucose metabolism in GP-Tag Tg mice. *A*: fasting blood glucose levels in 15-wk-old male Tg (black bar) and in non (open bar); n = 7–10. *B*: glucose tolerance tests in 15-wk-old male GP-Tag Tg mice (■) and in their nontransgenic littermates (◇); n = 6–11. *C*: insulin tolerance tests in male GP-Tag Tg mice (■) and in their nontransgenic littermates (◇); n = 5–8. *D*: serum insulin levels at basal, at 2 min, and at 30 min after intraperitoneal glucose injection in 15-wk-old male GP-Tag Tg mice (black bars) and in their nontransgenic littermates (open bars); n = 7–8. *E* and *F*: the mRNA (*E*) and the protein levels (*F*) of insulin in the pancreata of 15-wk-old male Tg mice (black bars) and in their non littermates (open bars); n = 6–8. $^*P < 0.05$, $^{**}P < 0.01$ compared with nontransgenic littermates.

sion, the amount of ghrelin production per cell was low. However, since the cell number was extremely increased, the net product by stomach was eventually elevated.

Several lines of evidence suggest that the GH-IGF-I axis is suppressed in the decreased GHS-R signaling state (28, 32). It has not yet been clear, however, whether chronic elevation of ghrelin within the physiological range could stimulate the GH-IGF-I axis. In this study, we found that adult GP-Tag Tg mice with elevated circulating ghrelin level showed elevated serum IGF-I level. Serum IGF-I level is regulated not only by GH but also by nutritional status. Malnutrition suppresses serum IGF-I level, whereas overnutrition elevates it (16). Since the nutritional state of GP-Tag Tg mice was poor because of decreased food intake, the elevated serum IGF-I levels in adult GP-Tag Tg mice are considered not to be due to overnutrition but to be due to activation of GH-IGF-I axis. Our findings indicate that chronic elevation of circulating ghrelin within the physiological range can activate the GH-IGF-I axis. As far as we know, this is the first report demonstrating that increased levels of circulating ghrelin within the physiological range can elevate serum IGF-I levels in rodent.

The GH-releasing action of ghrelin requires GHRH (11), and when coadministered, synergistic effects can be observed (13). Since GH responses to GHRH tended to be enhanced in adult GP-Tag Tg, the activation of the GH-IGF-I axis in GP-Tag Tg may be in part due to potentiation of the GH-releasing effect of GHRH. When the mRNA levels of components of GH regulation in pituitary and hypothalamus of GP-Tag Tg mice were investigated, an elevation of the pituitary GHS-R mRNA level was found. It is not clear whether this elevation of GHS-R mRNA in the pituitary contributes to the activated GH-IGF-I axis, since the GH response to ghrelin was not changed in GP-Tag Tg mice. At least these findings indicate that desensitization of GH secretion to ghrelin or downregulation of GHS-R did not occur by chronic elevation of circulating ghrelin in GP-Tag Tg mice.

Adult GP-Tag Tg mice exhibited high glucose level in the basal state and by the glucose tolerance test. Although insulin production was not decreased in the pancreata of GP-Tag Tg mice, insulin secretion after glucose load was significantly attenuated. Since the insulin sensitivity of GP-Tag Tg mice was not reduced, the glucose intorelance in GP-Tag Tg mice was due mainly to the decreased insulin secretion. Given that GP-Tag Tg mice have gastric tumors, there is a possibility that the glucose intorelance is due to the tumors. However, the glucose intolerance observed in malignancy is due mainly to insulin resistance (8, 15), which may be evoked by cytokines (22, 24, 27). Since the glucose intolerance of GP-Tag Tg mice was caused mainly by decreased insulin secretion, it seems not to be the case. It has been reported that acute injection of ghrelin induces suppression of insulin secretion in rodents and humans (6, 30). Our findings suggest that chronic elevation of circulating ghrelin within the physiological range leads to glucose intorelance by suppressing insulin secretion.

There have been several reports regarding ghrelin-producing tumors (9, 17, 36, 37). Most of the cases did not present

elevated plasma ghrelin levels except for a few cases. A malignant ghrelinoma case reported by Tsolakis et al. (36) showed elevated plasma ghrelin level. This patient maintained his weight despite progression of the tumor, a symptom that might be linked to the elevated ghrelin level. During the clinical course, he developed severe diabetes mellitus, which is consistent with the phenotype of GP-Tag Tg mice. GH and IGF-I levels were normal in this case. A pancreatic ghrelinoma case reported by Corbetta et al. (9) also showed normal GH and IGF-I levels despite elevated plasma ghrelin level. In contrast to these human ghrelinoma cases, GP-Tag Tg mice showed elevated IGF-I levels. The cause of the difference in the GH-IGF-I levels between our mice and these human ghrelinoma cases is unclear. Since the first case mentioned above was a malignant gastric ghrelinoma with liver metastasis, and the second case was of pancreatic origin, plasma ghrelin level might be elevated without any physiological regulation in these cases, although detailed plasma ghrelin level changes were not documented. Considering that the physiological regulation of ghrelin secretion was kept in GP-Tag Tg mice, the circadian rhythm may be needed for ghrelin to keep stimulating the GH-IGF-I axis. Indeed, several reports have shown that chronic treatment of ghrelin attenuates GH response both in vivo and in vitro (35, 39) and that in vitro treatment of pituitary with ghrelin results in decreased GHS-R mRNA levels (21). Further case studies will be required to reveal the relationship between plasma ghrelin levels and the GH-IGF-I axis in human ghrelinoma patients.

The limitation of this study is that the assessment of orexigenic action of ghrelin is difficult in this mouse model since stomach walls of GP-Tag Tg mice gradually become hypertrophic after 9 wk of age, which might affect the feeding behavior. Indeed, GP-Tag Tg mice exhibited decreased food intake and weight reduction despite the elevated plasma ghrelin levels. The hypothalamic mRNA levels of NPY and AgRP, which mediate the orexigenic action of ghrelin (7, 31), were not upregulated in GP-Tag Tg mice. There is a possibility that desensitization of GHS-R to chronic elevated ghrelin may be a cause of the lack of activation of these neurons besides the hypertrophy of the stomach wall. However, hypothalamic mRNA level of GHS-R was not changed. Furthermore, the food intake induced by acute ghrelin administration in GP-Tag Tg mice was comparable with control. These results may not support the idea of desensitization. Leptin and ghrelin have opposing effects on food intake. We examined whether plasma leptin levels of GP-Tag Tg mice were elevated as a compensation for the chronically elevated plasma ghrelin levels, which may cause anorexia. However, the leptin levels were decreased, provably reflecting the decreased fat mass of GP-Tag Tg mice.

In summary, we developed a mouse model of ghrelinoma, GP-Tag Tg mice, in which ghrelin concentrations were significantly elevated in adulthood. These GP-Tag Tg mice exhibited elevated IGF-I levels despite poor nutrition and glucose intolerance due to decreased insulin secretion. These characteristic features of this ghrelinoma mouse could be a guide to diagnose ghrelinoma.

ACKNOWLEDGMENTS

We thank Chieko Ishimoto and Chinami Shiraiwa for excellent technical assistance.

GRANTS

This study was supported by funds from the Ministry of Education, Culture, Sports, Science, and Technology of Japan and the Ministry of Health, Labour, and Welfare of Japan, a research grant from the Program for Promotion of Fundamental Studies in Health Sciences of the National Institute of Biomedical Innovation, and the Takeda Scientific Foundation in Japan.

REFERENCES

1. **Akamizu T, Shinomiya T, Irako T, Fukunaga M, Nakai Y, Kangawa K.** Separate measurement of plasma levels of acylated and desacyl ghrelin in healthy subjects using a new direct ELISA assay. *J Clin Endocrinol Metab* 90: 6–9, 2005.
2. **Ariyasu H, Takaya K, Iwakura H, Hosoda H, Akamizu T, Arai Y, Kangawa K, Nakao K.** Transgenic mice overexpressing des-acyl ghrelin show small phenotype. *Endocrinology* 146: 355–364, 2005.
3. **Ariyasu H, Takaya K, Tagami T, Ogawa Y, Hosoda K, Akamizu T, Suda M, Koh T, Natsui K, Toyooka S, Shirakami G, Usui T, Shimatsu A, Doi K, Hosoda H, Kojima M, Kangawa K, Nakao K.** Stomach is a major source of circulating ghrelin, and feeding state determines plasma ghrelin-like immunoreactivity levels in humans. *J Clin Endocrinol Metab* 86: 4753–4758, 2001.
4. **Asakawa A, Inui A, Fujimiya M, Sakamaki R, Shinfuku N, Ueta Y, Meguid MM, Kasuga M.** Stomach regulates energy balance via acylated ghrelin and desacyl ghrelin. *Gut* 54: 18–24, 2005.
5. **Bewick GA, Kent A, Campbell D, Patterson M, Ghatei MA, Bloom SR, Gardiner JV.** Mice with hyperghrelinemia are hyperphagic and glucose intolerant and have reduced leptin sensitivity. *Diabetes* 58: 840–846, 2009.
6. **Broglio F, Arvat E, Benso A, Gottero C, Muccioli G, Papotti M, van der Lely AJ, Deghenghi R, Ghigo E.** Ghrelin, a natural GH secretagogue produced by the stomach, induces hyperglycemia and reduces insulin secretion in humans. *J Clin Endocrinol Metab* 86: 5083–5086, 2001.
7. **Chen HY, Trumbauer ME, Chen AS, Weingarth DT, Adams JR, Frazier EG, Shen Z, Marsh DJ, Feighner SD, Guan XM, Ye Z, Nargund RP, Smith RG, Van der Ploeg LH, Howard AD, MacNeil DJ, Qian S.** Orexigenic action of peripheral ghrelin is mediated by neuropeptide Y and agouti-related protein. *Endocrinology* 145: 2607–2612, 2004.
8. **Copeland GP, Leinster SJ, Davis JC, Hipkin LJ.** Insulin resistance in patients with colorectal cancer. *Br J Surg* 74: 1031–1035, 1987.
9. **Corbetta S, Peracchi M, Cappiello V, Lania A, Lauri E, Vago L, Beck-Peccoz P, Spada A.** Circulating ghrelin levels in patients with pancreatic and gastrointestinal neuroendocrine tumors: identification of one pancreatic ghrelinoma. *J Clin Endocrinol Metab* 88: 3117–3120, 2003.
10. **Date Y, Kojima M, Hosoda H, Sawaguchi A, Mondal MS, Suganuma T, Matsukura S, Kangawa K, Nakazato M.** Ghrelin, a novel growth hormone-releasing acylated peptide, is synthesized in a distinct endocrine cell type in the gastrointestinal tracts of rats and humans. *Endocrinology* 141: 4255–4261, 2000.
11. **Dimaraki EV, Jaffe CA.** Role of endogenous ghrelin in growth hormone secretion, appetite regulation and metabolism. *Rev Endocr Metab Disord* 7: 237–249, 2006.
12. **Gutierrez JA, Solenberg PJ, Perkins DR, Willency JA, Knierman MD, Jin Z, Witcher DR, Luo S, Onyia JE, Hale JE.** Ghrelin octanoylation mediated by an orphan lipid transferase. *Proc Natl Acad Sci USA* 105: 6320–6325, 2008.
13. **Hataya Y, Akamizu T, Takaya K, Kanamoto N, Ariyasu H, Saijo M, Moriyama K, Shimatsu A, Kojima M, Kangawa K, Nakao K.** A low dose of ghrelin stimulates growth hormone (GH) release synergistically with GH-releasing hormone in humans. *J Clin Endocrinol Metab* 86: 4552, 2001.
14. **Hosoda H, Kojima M, Matsuo H, Kangawa K.** Ghrelin and des-acyl ghrelin: two major forms of rat ghrelin peptide in gastrointestinal tissue. *Biochem Biophys Res Commun* 279: 909–913, 2000.
15. **Isaksson B, Strommer L, Friess H, Buchler MW, Herrington MK, Wang F, Zierath JR, Wallberg-Henriksson H, Larsson J, Permert J.** Impaired insulin action on phosphatidylinositol 3-kinase activity and glucose transport in skeletal muscle of pancreatic cancer patients. *Pancreas* 26: 173–177, 2003.
16. **Iwakura H, Akamizu T, Ariyasu H, Irako T, Hosoda K, Nakao K, Kangawa K.** Effects of ghrelin administration on decreased growth hormone status in obese animals. *Am J Physiol Endocrinol Metab* 293: E819–E825, 2007.

17. **Iwakura H, Hosoda K, Doi R, Komoto I, Nishimura H, Son C, Fujikura J, Tomita T, Takaya K, Ogawa Y, Hayashi T, Inoue G, Akamizu T, Hosoda H, Kojima M, Kangawa K, Imamura M, Nakao K.** Ghrelin expression in islet cell tumors: augmented expression of ghrelin in a case of glucagonoma with multiple endocrine neoplasm type I. *J Clin Endocrinol Metab* 87: 4885–4888, 2002.
18. **Iwakura H, Hosoda K, Son C, Fujikura J, Tomita T, Noguchi M, Ariyasu H, Takaya K, Masuzaki H, Ogawa Y, Hayashi T, Inoue G, Akamizu T, Hosoda H, Kojima M, Itoh H, Toyokuni S, Kangawa K, Nakao K.** Analysis of rat insulin II promoter-ghrelin transgenic mice and rat glucagon promoter-ghrelin transgenic mice. *J Biol Chem* 280: 15247–15256, 2005.
19. **Kanamoto N, Akamizu T, Tagami T, Hataya Y, Moriyama K, Takaya K, Hosoda H, Kojima M, Kangawa K, Nakao K.** Genomic structure and characterization of the 5′-flanking region of the human ghrelin gene. *Endocrinology* 145: 4144–4153, 2004.
20. **Kojima M, Hosoda H, Date Y, Nakazato M, Matsuo H, Kangawa K.** Ghrelin is a growth-hormone-releasing acylated peptide from stomach. *Nature* 402: 656–660, 1999.
21. **Luque RM, Kineman RD, Park S, Peng XD, Gracia-Navarro F, Castano JP, Malagon MM.** Homologous and heterologous regulation of pituitary receptors for ghrelin and growth hormone-releasing hormone. *Endocrinology* 145: 3182–3189, 2004.
22. **Makino T, Noguchi Y, Yoshikawa T, Doi C, Nomura K.** Circulating interleukin 6 concentrations and insulin resistance in patients with cancer. *Br J Surg* 85: 1658–1662, 1998.
23. **Masuda Y, Tanaka T, Inomata N, Ohnuma N, Tanaka S, Itoh Z, Hosoda H, Kojima M, Kangawa K.** Ghrelin stimulates gastric acid secretion and motility in rats. *Biochem Biophys Res Commun* 276: 905–908, 2000.
24. **McCall JL, Tuckey JA, Parry BR.** Serum tumour necrosis factor alpha and insulin resistance in gastrointestinal cancer. *Br J Surg* 79: 1361–1363, 1992.
25. **Nagaya N, Kojima M, Uematsu M, Yamagishi M, Hosoda H, Oya H, Hayashi Y, Kangawa K.** Hemodynamic and hormonal effects of human ghrelin in healthy volunteers. *Am J Physiol Regul Integr Comp Physiol* 280: R1483–R1487, 2001.
26. **Nakazato M, Murakami N, Date Y, Kojima M, Matsuo H, Kangawa K, Matsukura S.** A role for ghrelin in the central regulation of feeding. *Nature* 409: 194–198, 2001.
27. **Noguchi Y, Yoshikawa T, Marat D, Doi C, Makino T, Fukuzawa K, Tsuburaya A, Satoh S, Ito T, Mitsuse S.** Insulin resistance in cancer patients is associated with enhanced tumor necrosis factor-alpha expression in skeletal muscle. *Biochem Biophys Res Commun* 253: 887–892, 1998.
28. **Pantel J, Legendre M, Cabrol S, Hilal L, Hajaji Y, Morisset S, Nivot S, Vie-Luton MP, Grouselle D, de Kerdanet M, Kadiri A, Epelbaum J, Le Bouc Y, Amselem S.** Loss of constitutive activity of the growth hormone secretagogue receptor in familial short stature. *J Clin Invest* 116: 760–768, 2006.
29. **Reed JA, Benoit SC, Pfluger PT, Tschöp MH, D'Alessio DA, Seeley RJ.** Mice with chronically increased circulating ghrelin develop age-related glucose intolerance. *Am J Physiol Endocrinol Metab* 294: E752–E760, 2008.
30. **Reimer MK, Pacini G, Ahren B.** Dose-dependent inhibition by ghrelin of insulin secretion in the mouse. *Endocrinology* 144: 916–921, 2003.
31. **Shintani M, Ogawa Y, Ebihara K, Aizawa-Abe M, Miyanaga F, Takaya K, Hayashi T, Inoue G, Hosoda K, Kojima M, Kangawa K, Nakao K.** Ghrelin, an endogenous growth hormone secretagogue, is a novel orexigenic peptide that antagonizes leptin action through the activation of hypothalamic neuropeptide Y/Y1 receptor pathway. *Diabetes* 50: 227–232, 2001.
32. **Shuto Y, Shibasaki T, Otagiri A, Kuriyama H, Ohata H, Tamura H, Kamegai J, Sugihara H, Oikawa S, Wakabayashi I.** Hypothalamic growth hormone secretagogue receptor regulates growth hormone secretion, feeding, and adiposity. *J Clin Invest* 109: 1429–1436, 2002.
33. **Tack J, Depoortere I, Bisschops R, Delporte C, Coulie B, Meulemans A, Janssens J, Peeters T.** Influence of ghrelin on interdigestive gastrointestinal motility in humans. *Gut* 55: 327–333, 2006.
34. **Takaya K, Ariyasu H, Kanamoto N, Iwakura H, Yoshimoto A, Harada M, Mori K, Komatsu Y, Usui T, Shimatsu A, Ogawa Y, Hosoda K, Akamizu T, Kojima M, Kangawa K, Nakao K.** Ghrelin strongly stimulates growth hormone release in humans. *J Clin Endocrinol Metab* 85: 4908–4911, 2000.
35. **Thompson NM, Davies JS, Mode A, Houston PA, Wells T.** Pattern-dependent suppression of growth hormone (GH) pulsatility by ghrelin and GH-releasing peptide-6 in moderately GH-deficient rats. *Endocrinology* 144: 4859–4867, 2003.
36. **Tsolakis AV, Portela-Gomes GM, Stridsberg M, Grimelius L, Sundin A, Eriksson BK, Oberg KE, Janson ET.** Malignant gastric ghrelinoma with hyperghrelinemia. *J Clin Endocrinol Metab* 89: 3739–3744, 2004.
37. **Volante M, Allia E, Gugliotta P, Funaro A, Broglio F, Deghenghi R, Muccioli G, Ghigo E, Papotti M.** Expression of ghrelin and of the GH secretagogue receptor by pancreatic islet cells and related endocrine tumors. *J Clin Endocrinol Metab* 87: 1300–1308, 2002.
38. **Wei W, Qi X, Reed J, Ceci J, Wang HQ, Wang G, Englander EW, Greeley GH Jr.** Effect of chronic hyperghrelinemia on ingestive action of ghrelin. *Am J Physiol Regul Integr Comp Physiol* 290: R803–R808, 2006.
39. **Yamazaki M, Nakamura K, Kobayashi H, Matsubara M, Hayashi Y, Kangawa K, Sakai T.** Regulational effect of ghrelin on growth hormone secretion from perifused rat anterior pituitary cells. *J Neuroendocrinol* 14: 156–162, 2002.
40. **Yang J, Brown MS, Liang G, Grishin NV, Goldstein JL.** Identification of the acyltransferase that octanoylates ghrelin, an appetite-stimulating peptide hormone. *Cell* 132: 387–396, 2008.
41. **Zhang W, Chai B, Li JY, Wang H, Mulholland MW.** Effect of des-acyl ghrelin on adiposity and glucose metabolism. *Endocrinology* 149: 4710–4716, 2008.

The Journal of Immunology

Suppression of Experimental Autoimmune Encephalomyelitis by Ghrelin

Michael-Mark Theil, Sachiko Miyake, Miho Mizuno, Chiharu Tomi, J. Ludovic Croxford, Hiroshi Hosoda, Julia Theil, Stephan von Hörsten, Hiroaki Yokote, Asako Chiba, Youwei Lin, Shinji Oki, Takashi Akamizu, Kenji Kangawa and Takashi Yamamura

J. Immunol. 2009;183;2859-2866; originally published online Jul 20, 2009;
doi:10.4049/jimmunol.0803362
http://www.jimmunol.org/cgi/content/full/183/4/2859

The Journal of Immunology is published twice each month by The American Association of Immunologists, Inc., 9650 Rockville Pike, Bethesda, MD 20814-3994.

Print ISSN: 0022-1767 Online ISSN: 1550-6606.

Suppression of Experimental Autoimmune Encephalomyelitis by Ghrelin[1]

Michael-Mark Theil,*† Sachiko Miyake,[2]* Miho Mizuno,* Chiharu Tomi,* J. Ludovic Croxford,* Hiroshi Hosoda,‡ Julia Theil,*† Stephan von Hörsten,†§ Hiroaki Yokote,* Asako Chiba,* Youwei Lin,* Shinji Oki,* Takashi Akamizu,¶ Kenji Kangawa,¶ and Takashi Yamamura[2]*

Ghrelin is a recently identified gastric hormone that displays strong growth hormone-releasing activity mediated by the growth hormone secretagogue receptor. While this unique endogenous peptide participates in the regulation of energy homeostasis, increases food intake, and decreases energy expenditure, its ability to inhibit the production of proinflammatory cytokines in vitro indicates its role in the regulation of inflammatory process in vivo. Here we examine the effect of exogenous ghrelin on the development of experimental autoimmune encephalomyelitis (EAE), a representative model of multiple sclerosis. In the C57BL/6 mouse model of EAE induced by sensitization to myelin oligodendrocyte glycoprotein 35–55 peptide, we found that alternate-day s.c. injections of ghrelin (5 μg/kg/day) from day 1 to 35 significantly reduced the clinical severity of EAE. The suppression of EAE was accompanied by reduced mRNA levels of proinflammatory cytokines such as TNF-α, IL-1β, and IL-6 in the spinal cord cellular infiltrates and microglia from ghrelin-treated mice at the peak of disease, suggesting the role of ghrelin as an antiinflammatory hormone. Consistently, ghrelin significantly suppressed the production of proinflammatory cytokines in LPS-stimulated microglia in vitro. These results shed light on the new role of ghrelin in the regulation of inflammation with possible implications for management of human diseases. ***The Journal of Immunology,*** **2009, 183: 2859–2866.**

Small synthetic compounds, referred to as growth hormone (GH)[3] secretagogues (GHS), have been known to stimulate GH release, working through a G protein-coupled receptor called GHS receptor (GHS-R) (1–3). It is now established that a new endogenous peptide, ghrelin, discovered in rat gastric extracts, is an endogenous ligand for GHS-R and is involved in the regulation of GH release. Ghrelin is a 28-aa polypeptide with an essential *n*-octanoyl modification on serine at position 3 (4). Although ghrelin is predominantly secreted from mucosal endocrine cells of stomach, it is widely distributed in various organs, including lymphoid tissues (5, 6). Furthermore, it is measurable in the systemic circulation, indicating its hormonal nature (7).

Ghrelin does not only stimulate GH release, but it also increases food intake, regulates energy homeostasis, and decreases energy expenditure by lowering the catabolism of fat (4, 8, 9). Because of its orexigenic and adipogenic character, ghrelin may be potentially useful for the treatment of anorexia and cachexia (10, 11). Although the precise mechanisms remain to be clarified, the orexigenic activities of ghrelin may be mediated by another feeding regulatory hormone neuropeptide Y (NPY) via stimulation of Y1 and Y5 receptors (12). Furthermore, the antagonistic effect of ghrelin on leptin-induced decrease of food intake seems to be mediated by ghrelin-induced release of NPY and subsequent stimulation of the Y1 receptor (13).

Ghrelin has been shown to exhibit antiinflammatory functions against T cells and macrophages in vitro (14–16). The potential activity of ghrelin as antiinflammatory reagent in vivo was shown in several animal models, including bowel disease (17), arthritis (16, 18), sepsis, and endotoxemia (16, 19, 20). Here we report that s.c. injections of ghrelin could significantly attenuate the clinical severity of the representative model of experimental autoimmune encephalomyelitis (EAE) induced in C57BL/6 (B6) mice by sensitization against myelin oligodendrocyte glycoprotein $(MOG)_{35-55}$ peptide. Furthermore, we demonstrate that in vivo treatment with ghrelin significantly suppressed the mRNA levels of the proinflammatory cytokines TNF-α, IL-1β, and IL-6 in microglia and infiltrating T cells derived from the spinal cords of ghrelin-treated mice. Finally, we confirm that LPS-stimulated microglia and monocytes produced lower amounts of proinflammatory cytokines when they were pretreated with ghrelin in vitro. In conclusion, the present study indicates the potential use of ghrelin as an antiinflammatory drug to control human CNS pathology.

Materials and Methods

Mice and reagents

We used female B6 mice (CLEA Japan) between 6 and 10 wk of age in specific pathogen-free conditions. Animal care and use were in accordance

*Department of Immunology, National Institute of Neuroscience, National Centre of Neurology and Psychiatry, Tokyo, Japan; †Department of Functional and Applied Anatomy, Hannover Medical School, Hannover, Germany: ‡Department of Biochemistry, National Cardiovascular Center Research Institute, Fujishirodai, Suita, Osaka, Japan; §Experimental Therapy, Franz-Penzoldt-Center, Friedrich-Alexander-University Erlangen-Nürnberg, Erlangen, Germany; and ¶Ghrelin Research Project, Translational Research Center, Kyoto University Faculty of Medicine, Kyoto, Japan

Received for publication October 14, 2008. Accepted for publication June 9, 2009.

The costs of publication of this article were defrayed in part by the payment of page charges. This article must therefore be hereby marked *advertisement* in accordance with 18 U.S.C. Section 1734 solely to indicate this fact.

[1] This work was supported by the grants from the Ministry of Health, Labor, and Welfare of Japan, the Program for Promotion of Fundamental Studies in Health Sciences of the National Institute of Biomedical Innovation (NIBIO), and the Ministry of Education, Science, Culture, Sports, and Technology of Japan.

[2] Address correspondence and reprint requests to Dr. Sachiko Miyake or Dr. Takashi Yamamura, Department of Immunology, National Institute of Neuroscience, National Centre of Neurology and Psychiatry, 4-1-1 Ogawahigashi, Kodaira, Tokyo 187-8502. E-mail address: miyake@ncnp.go.jp or yamamura@ncnp.go.jp

[3] Abbreviations used in this paper: GH, growth hormone; EAE, experimental autoimmune encephalomyelitis; GHS, growth hormone secretagogue; GHS-R, growth hormone secretagogue receptor; LN, lymph node; MOG, myelin oligodendrocyte glycoprotein; NPY, neuropeptide Y.

www.jimmunol.org/cgi/doi/10.4049/jimmunol.0803362

Table I. *Amino acid sequence of mouse ghrelin and des-acyl ghrelin*

Peptide	Amino Acid Sequence[a]	Ser^3 acylation	Reference
Ghrelin	GSSFLSPEHQKAQQRKESKKPPAKLQPR	*n*-Octanoicacid	(4)
Des-acyl ghrelin	GSSFLSPEHQKAQQRKESKKPPAKLQPR		(7)

[a] The underlined letter S represents the third serine (Ser^3).

with institutional guidelines. Animal experiments were approved by our institutional review committee. Rat MOG_{35-55} (amino acid sequence MEVGWYRSPFSRVVHLYRNGK) was synthesized at Toray Research Center (Tokyo, Japan). Ghrelin and des-acyl ghrelin (Table I) were synthesized as previously described (4, 7).

Immunization and clinical assessment of EAE

We immunized mice (n = 5–15 per group) s.c. in the tail base with 100 μg of MOG_{35-55}-peptide dissolved in 0.1 ml of PBS and 0.1 ml of CFA containing 1 mg of *M. tuberculosis* H37Ra (Difco). Shortly after immunization and 48 h later, the mice were injected i.p. with 200 ng of pertussis toxin (List Biological Laboratories). Clinical scores of EAE were daily assigned as follows: 0, normal; 1, weakness of the tail and/or paralysis of the distal half of the tail; 2, loss of tail tonicity; 3, partial hind limb paralysis; 4, complete hind limb paralysis; 5, forelimb paralysis or moribund; 6, death. The cumulative scores were calculated for individual mice by summing up the daily scores.

Administration of ghrelin and des-acyl ghrelin

For EAE treatment, we s.c. injected ghrelin and des-acyl ghrelin diluted in 0.9% saline. In the first series of experiments, mice were injected with ghrelin or des-acyl ghrelin at doses of 0.5, 5, or 50 μg/kg every other day for 35 days. Sham-treated animals were injected with 0.9% saline (standard protocol). In the next experiment, we injected the mice with 5 μg/kg ghrelin every day from day 1 to 10 (induction phase treatment) or from day 11 to 20 (effector phase treatment) and in-between with 0.9% saline. The controls were injected every day from day 1 to 20 with 0.9% saline (alternative protocol).

Assessment of histological EAE

To evaluate the histological manifestations of EAE, we treated mice with 5 μg/kg ghrelin or 0.9% saline following the standard protocol and sacrificed them on day 17 postimmunization. The spinal cords were removed and fixed in buffered formalin. They were embedded in paraffin, sectioned, and stained with H&E and Luxol fast blue for histopathological analysis.

Flow cytometry and isolation of mononuclear cells from the CNS

B6 mice were challenged for EAE, treated following the standard protocol with 5 μg/kg ghrelin or 0.9% saline and sacrificed on day 17 postimmunization. We removed spleen, lymph nodes (LN), and thymus as well as spinal cord from the ghrelin- and saline-treated mice for flow cytometer analysis. Single-cell suspensions were prepared according to standard methods. The spinal cord cell suspensions were centrifuged at 200 × g for 10 min and resuspended in 4 ml of 70% isotonic Percoll (Amersham Biosciences)/PBS and overlaid by equal volumes of 37% and 30% isotonic Percoll. The gradient was centrifuged at 500 × g for 15 min and the mononuclear cells were harvested from the 37%–70% interface, washed, and counted. The cells were stained for 5 min with anti-FcRγ III/II mAb (BD Pharmingen), washed, and labeled with the following mAbs for surface phenotype analysis: FITC-CD4 mAb, FITC-CD19 mAb, PE-CD8a mAb, PE-NK1.1 mAb, PE-CD25 mAb, allophycocyanin-FOXP3, and PerCP-Cy5.5-CD3e mAb (BD Pharmingen) and FITC-F4/80 mAb (Dainihon Seiyaku). The cytofluorometric analysis was performed using a FACSCalibur operated by CellQuest software (BD Biosciences).

Cytokine and cell proliferation assay

MOG_{35-55}-immunized B6 mice were treated s.c. with 5 μg/kg/day of ghrelin or 0.9% saline every day from day 1 to 10. The LN cells were collected on day 11 after immunization and suspended in our standard lymphocyte culture medium (RPMI 1640 supplemented with 5 × 10^{-5} M 2-ME, 2 mM L-glutamine, 100 U/ml penicillin/streptomycin) added with 1% syngeneic mouse serum. The cells were cultured in 96-well round-bottom plates at 1 × 10^6/well for 72 h in the presence of 100 μg/ml MOG_{35-55}. Levels of IFN-γ, IL-17, and IL-4 in the supernatant were determined by using a sandwich ELISA. Proliferative responses were measured using a Beta-1205 counter (Pharmacia) to detect the incorporation of [^{3}H]thymidine (1 μCi/well) for the final 16 h of culture.

Evaluation of encephalitogenic T cell induction in B6 mice treated with ghrelin

To evaluate whether in vivo ghrelin treatment may affect the induction of encephalitogenic T cells after immunization with MOG_{35-55}, we evaluated the ability of the lymphoid cells from ghrelin- or saline-treated mice to passively transfer EAE into naive recipients. Donor B6 mice were immunized with MOG_{35-55} and treated every day from day 1 to 10 with 5 μg/kg/day of ghrelin or 0.9% saline. We removed spleens and LN from the donor mice on day 11 and prepared lymphoid cell suspensions. The lymphoid cells were stimulated with MOG_{35-55} (33 μg/ml) in the standard medium added with FCS (10%) for 96 h and then we isolated the $CD4^+$ T cells for cell transfer by depletion of $CD8^+$, $CD19^+$, and $NK1.1^+$ cells. In brief, the MOG_{35-55}-stimulated total lymphoid cells were labeled with PE-CD8a mAb, PE-NK1.1 mAb, and PE-CD19 mAb (BD Pharmingen) for 30 min, washed, and incubated with anti-PE microbeads (Miltenyi Biotec) for 15 min. Using autoMACS (Miltenyi Biotec), we isolated $CD4^+$ T cells ($CD8^-$, $CD19^-$, and $NK1.1^-$ fraction) as a pass-through and suspended the cells in PBS. We injected 1.0 × 10^7 of the cells into the peritoneal cavity of syngeneic recipient mice that had been X-irradiated (550 rad) shortly before. We also injected 200 ng of pertussis toxin i.p. on the same day and 48 h later.

Reverse transcription and real-time PCR

To analyze the mechanism of ghrelin effects in vivo, we extracted total RNA from spinal cord, spleen, thymus, and LN samples using the RNeasy Mini Kit (Qiagen). The RNA was subjected to reverse transcription with the Advantage RT-for-PCR kit (BD Biosciences). Real-time PCR was conducted in the LightCycler quantitative PCR system (Roche Molecular Biochemicals) by using the LightCycler-FastStart DNS Master SYBR Green I kit (Roche Molecular Biochemicals). We followed the manufacturer's specification using 4 mM $MgCl_2$ and 1 pM primers. The primers used are as follows: TNF-α, CTGTGAAGGGAATGGGTGTT (sense) and GGT CACTGTCCCAGCATCTT (antisense); IL-1β, TGAAATGCCACCTTT TGACA (sense) and GTAGCTGCCACAGCTTCTCC (antisense); IL-6, TTCCATCCAGTTGCCTT–CTT (sense) and CAGAATTGCCATTGC ACAAC (antisense); TGF-β, TGCGCTTGCAGA–GATTAAAA (sense) and GCTGAATCGAAAGCCCTGTA (antisense); and HPRT, GTTGGA–TACAGGCCAGACTTTGTTG (sense) and GAGGGTAGGCTGGCCT ATAGGCT (antisense). Values are presented as the relative amount of transcript of each sample normalized to the housekeeping gene hypoxanthine phosphoribosyltransferase (HPRT).

In vitro effect of ghrelin on RAW 264.7 monocytes treated with LPS

To examine the effect of ghrelin on monocytes, RAW 264.7 monocytes (American Type Culture Collection) were suspended in the standard culture medium supplemented with 10% FCS and cultured in 96-well flat bottom plates at 1 × 10^5/well overnight. Various concentrations of ghrelin (10^{-6} M, 10^{-8} M, 10^{-10} M) were added to the culture and 1 h later the cells were stimulated with LPS (Sigma-Aldrich) at various doses (0.1, 1, 10 μg/ml). After 2 h of incubation at 37°C, supernatants were collected and the levels of TNF-α and IL-6 were detected by using a sandwich ELISA.

Isolation of microglial cells from the CNS

The spinal cords were incubated with 35 mg/ml Liberase Blendzyme 3 (Roche Molecular Biochemicals) and 0.1 mg/ml DNaseI (Roche Molecular Biochemicals) in RPMI 1640 medium at 37°C for 30 min. Mononuclear cells were isolated on 30%–80% discontinuous Percoll gradients and were stained with FITC-CD11b mAb, PE-CD45 mAb, and allophycocyanin-CD3 mAb (BD Pharmingen). $CD11b^{high}CD45^{high}$ macrophage cells, $CD11b^{int}CD45^{int}$ microglial cells, and $CD3^+$ T cells were isolated using

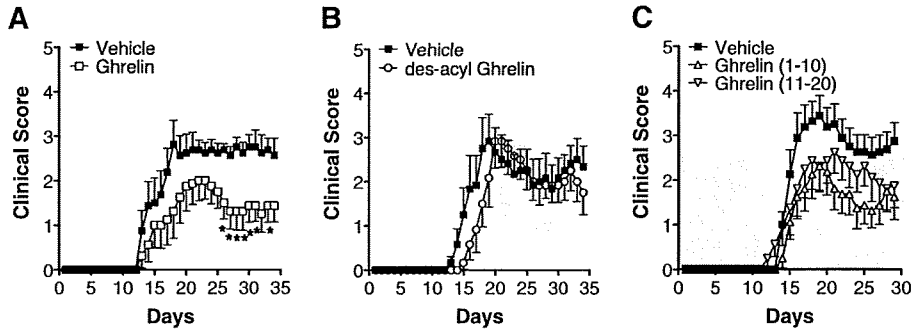

FIGURE 1. Effect of ghrelin on actively induced EAE. EAE was induced in female B6 mice (n = 8 in each group of the three experiments) by immunization with MOG_{35-55}. *A*, The mice were treated every other day starting at the day of immunization with 5 μg/kg ghrelin, while controls were administrated with the vehicle, 0.9% saline, alone. *B*, The mice were injected from day 1 every other day with 5 μg/kg des-acyl ghrelin, whereas controls were subjected to 0.9% saline injections. *C*, Following an alternative protocol, mice were treated from days 1–10 (induction phase treatment) or from days 11–20 (effector phase treatment) with 5 μg/kg ghrelin and in-between with 0.9% saline, while controls were treated every day with 0.9% saline injections. Data represent mean ± SEM. *, Significant differences between the groups ($p < 0.05$; Mann-Whitney U test).

FACSAria (BD Biosciences). The total RNA was extracted from the isolated cells and was subjected to reverse transcription and real-time PCR.

In vitro effect of ghrelin on microglia cells treated with LPS

Mononuclear cells were prepared from brains of untreated non-EAE mice incubated with Liberase Blendzyme 3 and DNase I as described above and were isolated on 40%–80% discontinuous Percoll gradients. Isolated cells were suspended in DMEM supplemented with 10% FCS and cultured in 96-well flat bottom plates at 2×10^5/well in the presence of ghrelin (10^{-6} M) overnight and later stimulated with LPS at different doses (0.01, 0.1 μg/ml). After 5 h of incubation at 37°C, supernatants were collected and the levels of TNF-α were detected by using a sandwich ELISA.

Statistical analysis

The differences in the clinical score between ghrelin-, des-acyl ghrelin-, and sham-treated groups were analyzed by the nonparametric Mann-Whitney U test. FACS analysis, real-time PCR, ELISA, and proliferation data were subjected to two-way ANOVA. In case of significant differences, a Fisher post hoc test was applied. Probability values of <0.05 were considered as statistically significant.

Results

Ghrelin inhibits EAE

To explore the modulatory effects of ghrelin on inflammatory demyelinating diseases, we employed a model of EAE actively induced in B6 mice with MOG_{35-55}. Although classical forms of EAE are typically characterized by acute paralysis followed by complete recovery, this EAE model shows persistent paralysis with partial recovery as a reflection of persistent inflammatory demyelination in the CNS (21, 22). In the first series of experiments, we injected 0.5, 5, or 50 μg/kg ghrelin to the mice every other day from day 1 to 35 postimmunization, while the control mice were injected with 0.9% saline. The results showed that the continuous injections of 5 μg/kg ghrelin suppressed most efficiently the clinical signs of EAE (Fig. 1*A*), whereas a lower (0.5 μg/kg) or a higher dose (50 μg/kg) showed only a marginal effect (data not shown). The treatment with 5 μg/kg ghrelin did not significantly alter either the onset or peak score of EAE. However, significant differences were noted in mean clinical score after day 25 postimmunization between the ghrelin-treated and the control mice (Fig. 1*A*).

Moreover, the effect of ghrelin on EAE was specific as des-acyl ghrelin, an acyl-modified ghrelin, which lacks the n-octanoic acid on the third serine, and consequently its binding ability to GHS-R (7) (Table I) had no modulatory effect on EAE at any concentration examined (Fig. 1*B* and Table II). Thus, the discrepant results obtained with ghrelin and des-acyl ghrelin indicate that ghrelin treatment would ameliorate the clinical course of EAE via activation of the GHS-R.

To further characterize the effects of ghrelin on EAE, we next examined if treatment lasting for a shorter duration may also be immunomodulatory in vivo. We injected 5 μg/kg ghrelin every day from day 1 to 10 postimmunization (roughly corresponding to the induction phase) or from day 11 to 20 (roughly corresponding to the effector phase). As shown in Fig. 1*C*, both protocols showed similar levels of disease suppression, although it was less notable than the continuous treatment from day 1 to 35 (Table II).

Ghrelin does not influence cellular infiltration into CNS

In the previous results on prophylactic or therapeutic treatment of EAE, clinical suppression of EAE was generally associated with a significant reduction of cellular infiltration in the CNS (23). To clarify if histological manifestation of EAE is also suppressed by ghrelin treatment, we treated MOG_{35-55}-immunized B6 mice with 5 μg/kg ghrelin or 0.9% saline every other day and prepared sections of spinal cords at the peak of disease (day 17 after immunization) (Fig. 2). Clinical signs were milder in the ghrelin-treated mice compared with saline-treated ones. However, histology of the spinal cord sections with H&E staining revealed equivalent levels of cellular infiltration in ghrelin- and saline-treated mice. To confirm this, we isolated mononuclear cells from spinal cords of the

Table II. *Clinical scores of EAE treated with ghrelin or des-acyl ghrelin following different treatment protocols*[a]

Treatment	Incidence	Mean Day of Onset ± SEM	Mean Maximal Score ± SEM	Mean Cumulative Score ± SEM
Vehicle[b]	8/8	16.38 ± 1.13	3.75 ± 0.33	55.44 ± 7.14
Ghrelin[b]	7/8	17.86 ± 1.30	3.29 ± 0.33	36.71 ± 9.99
Vehicle[b]	6/8	18.83 ± 2.55	3.67 ± 0.40	49.33 ± 12.99
Des-acyl ghrelin[b]	6/8	18.00 ± 0.71	3.80 ± 0.44	49.05 ± 8.09
Vehicle[c]	7/8	15.14 ± 0.51	4.43 ± 0.07	50.43 ± 3.10
Ghrelin (1–10)[c]	6/8	16.00 ± 0.73	3.17 ± 0.53	34.00 ± 7.25
Ghrelin (11–20)[c]	7/8	16.29 ± 1.25	3.50 ± 0.45	38.72 ± 8.79

[a] The table shows the results of three separate experiments (n = 8 mice in each group of the three experiments).

[b] After induction of EAE with MOG_{35-55}, mice were treated in two different experiments following the standard protocol of every other day s.c. treatment with 5 μg/kg ghrelin or 5 μg/kg des-acyl ghrelin. The controls were injected with 0.9% saline (vehicle).

[c] Following an alternative protocol, we treated the mice from days 1–10 (induction phase treatment) or from days 11–20 (effector phase treatment) with 5 μg/kg ghrelin and in-between with 0.9 % saline, while controls were injected every day with 0.9% saline only. Data represent mean ± SEM.

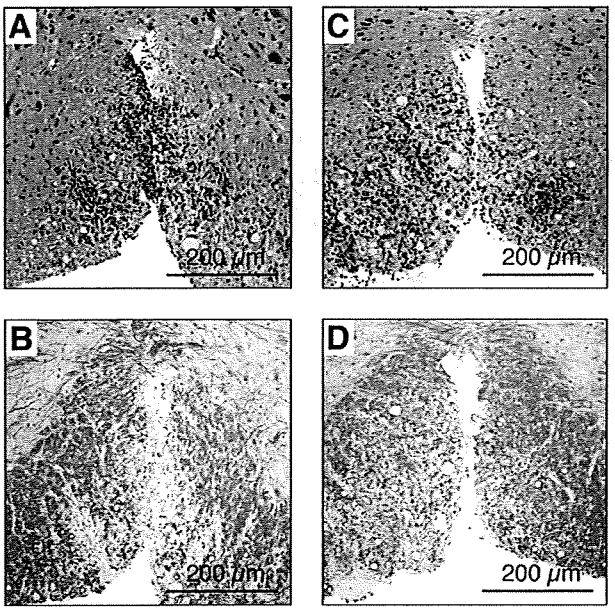

FIGURE 2. Histopathological assessment of the spinal cord of EAE mice. Spinal cords from EAE mice (n = 5/group) were removed on day 17 postimmunization as described in *Material and Methods*. The spinal cord sections from sham- (*A* and *B*) and ghrelin-treated (*C* and *D*) mice were stained in with H&E in the upper panels or Luxol fast blue in the lower ones. Representative sections are shown.

mice at the peak of disease and enumerated the number of the lymphoid cells. Notably, the total cell number was slightly elevated in the ghrelin-treated mice (1.40×10^6/mouse) compared with the saline-treated mice (1.05×10^6/mouse). To further analyze the effects of ghrelin on the formation of CNS inflammation, we evaluated the cellular composition of the CNS-derived lymphocytes by using FACS. Although there was a trend that $CD4^+$ and $CD8^+$ T cell numbers are increased in the lesions of ghrelin-treated mice as compared with saline-treated mice (Fig. 3*A*), it did not reach the level of statistic significance. It was also noted that ghrelin treatment did not alter the number of NK cells

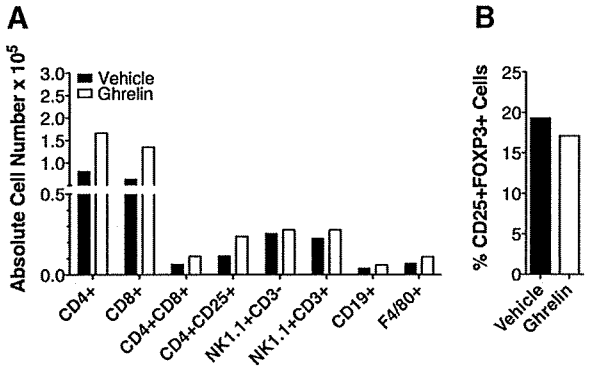

FIGURE 3. Quantification of spinal cord cellular infiltrates by flow cytometry. *A*, The cells were isolated from spinal cords of ghrelin- and sham-treated mice on day 17 postimmunization and subjected to flow cytometer analysis as described in *Materials and Methods*. Data are representative of two independent experiments and presented as absolute cell number (n = 8 mice/group in each experiment). *B*, The proportion of $CD25^+FOXP3^+$ cells in the $CD4^+$ T cell population isolated from spinal cord mononuclear cells was analyzed by flow cytometry 20 days after immunization. Data represent two independent experiments (n = 5).

Table III. *Cytokine production and proliferation of MOG_{35-55}-specific T cells after ghrelin treatment*[a]

Treatment	CPM ± SEM	Cytokine Production (pg/ml) INF-γ ± SEM	IL-17 ± SEM	IL-4 ± SEM
Vehicle	47,590 ± 10,988	2,087 ± 487	820 ± 211	ND
Ghrelin	36,663 ± 9,058	2,883 ± 615	674 ± 148	ND

[a] Mice were immunized with MOG_{35-55} and treated with 5 μg/kg ghrelin or 0.9% saline everyday from day 1 to 10 (n = 3/group). Popliteal and inguinal LN cells were harvested on day 11 after immunization and stimulated with 10 μg/ml MOG_{35-55}. CPM marks the proliferative response to MOG_{35-55}. The cytokines were measured in the supernatant by sandwich ELISA after 72 h of stimulation. Data represent mean ± SEM of duplicate samples from one out of three independent experiments. ND, Not detectable.

($NK1.1^+CD3^-$), NKT cells ($NK1.1^+CD3^+$), B cells ($CD19^+$), or macrophages ($F4/80^+$) in the spinal cord lesions. The proportions of $CD25^+FOXP3^+$ cells in the $CD4^+$ T cell population isolated from spinal cords were not altered in ghrelin-treated mice (Fig. 3*B*). In parallel, we also examined the composition of lymphoid cells obtained from spleen, LN, and thymus. Again, we could not reveal any significant change in the subsets of lymphocytes in ghrelin-treated mice (data not shown). Concordant with the histological findings, these data imply that ghrelin did not ameliorate clinical EAE by reducing the numbers of inflammatory cells in the CNS, but rather by regulating the inflammatory potential of the CNS infiltrates.

Ghrelin does not inhibit the induction of MOG_{35-55}-reactive T cells

To elucidate the immunomodulatory mechanism of ghrelin, we examined the cytokine production and proliferative response of draining LN cells to MOG_{35-55} that were obtained from MOG_{35-55}-sensitized mice treated for 10 days every day with ghrelin or saline. The LN cells were collected on day 11 after immunization and stimulated with MOG_{35-55} in vitro. Accordingly, we harvested the supernatant and measured the levels of IFN-γ, IL-17, and IL-4 by using ELISA. Although the IL-4 concentration was under the detection level, IFN-γ and IL-17 could be detected in the MOG_{35-55}-stimulated culture supernatant (Table III). There was no significant difference in the level of IFN-γ and IL-17 when we compared ghrelin-treated and saline-treated groups. Furthermore, ghrelin-treated mice did not differ from saline-treated mice in the proliferative response of the draining LN cells to MOG_{35-55}. We also examined the frequency of $CD4^+CD25^+$ $FOXP3^+$ regulatory T cells in the lymph nodes and spleens using flow cytometry and did not find significant differences between ghrelin-treated and saline-treated mice (data not shown). These results indicate that in vivo ghrelin treatment did not inhibit the induction of MOG_{35-55}-reactive T cells.

Ghrelin does not affect induction of pathogenic autoimmune T cells

To further confirm that MOG_{35-55}-reactive T cells are normally induced in ghrelin-treated mice, we evaluated if the ability of the MOG_{35-55}-sensitized lymphoid cells, obtained from MOG_{35-55}-immunized mice, to transfer EAE into naive mice could be affected by in vivo ghrelin treatment. To this aim, we immunized donor mice with MOG_{35-55} and treated them every day with ghrelin or saline from immunization up to day 10. Next day, we pooled lymphocytes from spleen and LN and cultured them in the presence of MOG_{35-55}. Three days later, $CD4^+$ T cells were purified and injected into recipient mice as described in *Materials and Methods*. It was theoretically possible that in vivo ghrelin treatment does not

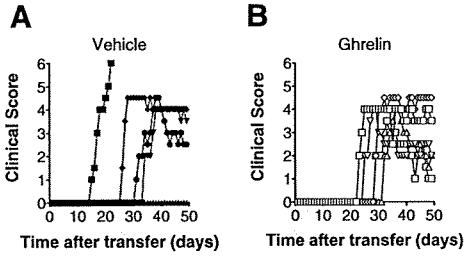

FIGURE 4. Effects of ghrelin treatment on the induction of encephalitogenic T cells. MOG_{35-55}-sensitized lymphoid cells were derived from MOG_{35-55}-immunized and (*A*) saline- or (*B*) ghrelin-treated mice (n = 15/group). The cells were stimulated with MOG_{35-55} and $CD4^+$ T cells were separated 3 days later for passive transfer of EAE into naive mice (n = 5/group). Data represent individual EAE score for each mouse.

inhibit induction of MOG_{35-55}-reactive T cells, but would prohibit the ability to cause EAE in vivo. In postulating that this could happen, $CD4^+$ T cells from ghrelin-treated donors should be less encephalitogenic than those from saline-treated mice. The results showed that transfer of activated $CD4^+$ T cells either derived from saline- or ghrelin-treated donors induced passive EAE in the recipients, showing approximately the same clinical course and severity (Fig. 4). Thus, it can be concluded that ghrelin treatment does not affect the induction of encephalitogenic MOG_{35-55}-reactive $CD4^+$ T cells.

Ghrelin decreases mRNA levels of proinflammatory cytokines in the CNS

After demonstrating that ghrelin does not suppress the infiltration of inflammatory cells in the spinal cord, we wondered whether the cytokine milieu in the ghrelin-treated mice could be significantly altered. To answer the question, we analyzed the mRNA levels of pro- and antiinflammatory cytokines (IFN-γ, TNF-α, IL-1β, IL-6, IL-4, IL-10, and TGF-β) in the spinal cord, spleen, LN, and thymus of ghrelin- and saline-treated mice at the peak of disease (day 17) by using quantitative PCR. Although ghrelin treatment had no effect on the mRNA levels of IL-4, IL-10, and IFN-γ in the spinal cord, spleen, LN, and thymus (data not shown), we found significantly reduced levels of TNF-α ($p < 0.0015$), IL-1β ($p < 0.025$), and IL-6 ($p < 0.025$) in the spinal cord of ghrelin-treated mice, compared with saline-treated ones (Fig. 5*A*). In contrast, the level of TGF-β showed a trend for slight elevation in the spinal cord. We also found a diminished level of TNF-α mRNA ($p < 0.0001$) in the spleen of ghrelin-treated mice (Fig. 5*B*), whereas we saw no significant change in any of the cytokines that we measured in LN or thymus of ghrelin-treated mice (Fig. 5, *C* and *D*). Because TNF-α, IL-1β, and IL-6 mRNAs were selectively down-regulated in the spinal cord, we suspected that monocytes could be potential target cells in the ghrelin-mediated EAE suppression. This idea was consistent with the fact that ghrelin treatment did not inhibit the induction of MOG_{35-55}-reactive T cells.

Ghrelin suppresses the proinflammatory cytokine production of LPS-stimulated monocytes

To verify the postulate that in vivo treatment with ghrelin may ameliorate EAE by targeting monocytes, we examined in vitro effects of ghrelin on the monocytic cell line RAW 264.7 that robustly produce proinflammatory cytokines when stimulated with LPS. The RAW 264.7 line cells were first exposed to various doses of ghrelin for 1 h and then stimulated with LPS. We harvested the supernatant 2 h later and measured the levels of TNF-α and IL-6 by ELISA. The results revealed that prior exposure to ghrelin

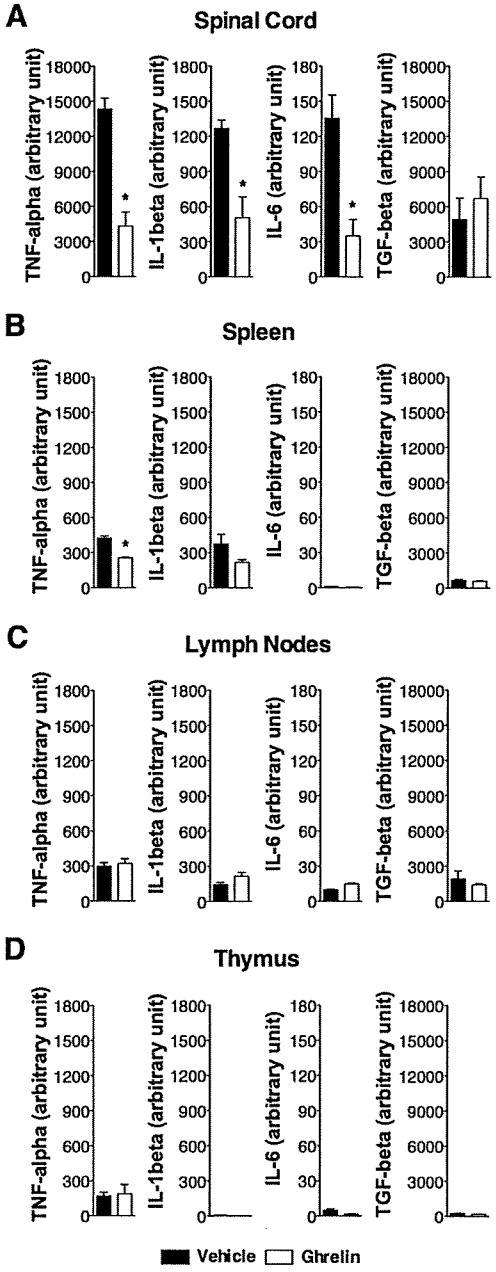

FIGURE 5. Proinflammatory cytokine mRNA expression during EAE in ghrelin-treated mice. Quantitative mRNA expression of proinflammatory cytokines in the spinal cord of MOG_{35-55}-immunized mice subjected to ghrelin or saline treatment on day 17 postimmunization (n = 5/group). Total mRNA was extracted from (*A*) spinal cord, (*B*) spleen, (*C*) LN, and (*D*) thymus. The TNF-α, IL-1β, IL-6, and TGF-β mRNA expression was measured by real-time PCR. Data are presented as relative amount of transcript normalized to HPRT. Data represent mean ± SEM. *, Significant differences between the groups ($p < 0.025$; two-way ANOVA).

would significantly suppress the production of TNF-α ($p < 0.02$) and IL-6 ($p < 0.05$) by LPS-stimulated RAW 264.7 cells in a dose-dependent manner (Fig. 6). The inhibitory effect of ghrelin was very potent, as in addition to the effects on LPS-stimulated monocytes, even the basal production of TNF-α ($p < 0.008$) and IL-6 ($p < 0.03$) was significantly reduced by in vitro ghrelin treatment. Given that in vivo treatment with ghrelin could suppress the

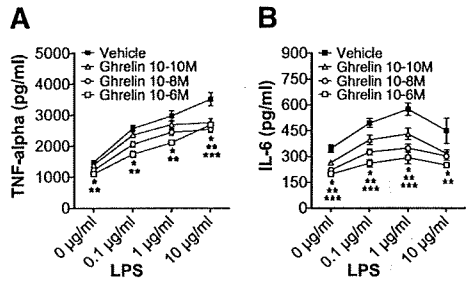

FIGURE 6. Effect of ghrelin on the proinflammatory cytokine production of LPS-stimulated monocytes. The monocytes were treated with various concentrations of ghrelin (10^{-6} M, 10^{-8} M, 10^{-10} M) 1 h before stimulation with 0.1, 1.0, and 10 µg/ml LPS. The (*A*) TNF-α and (*B*) IL-6 production was measured 2 h after LPS stimulation by sandwich ELISA. Data represent mean ± SEM of duplicate samples from one out of three independent experiments. Significant differences at 10^{-6}, 10^{-8}, and 10^{-10} M ($p < 0.05$; two-way ANOVA) are depicted as *, **, and ***, respectively.

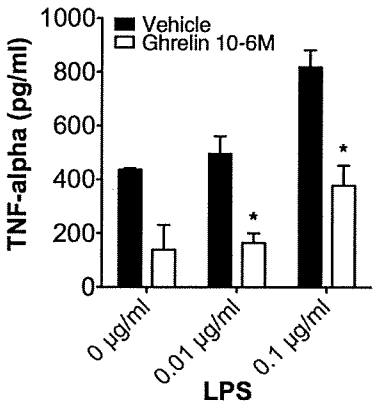

FIGURE 8. Effect of ghrelin on the proinflammatory cytokine production of LPS-stimulated microglia. The microglia cells were treated with ghrelin (10^{-6} M) overnight and later stimulated with 0.01 and 0.1 µg/ml LPS. Five hours after stimulation, the TNF-α production was measured using ELISA. Data represent mean ± SEM of duplicate samples from one out of two independent experiments. *, Significant differences between the groups ($p < 0.05$; two-way ANOVA).

development of EAE without altering histological EAE or T cell-derived cytokine balance, the ghrelin-mediated suppression of monocyte-produced TNF-α and IL-6 would strongly support the postulate that monocytes are the main target cells in ghrelin-mediated suppression of EAE.

Ghrelin inhibits the expression of proinflammatory cytokines in microglia

The proinflammatory cytokines are known to be produced not only by CNS-infiltrating macrophages but also by T cells and microglia in the course of EAE. To investigate which cells are important in the ghrelin-mediated suppression of EAE, we first examined the expression of proinflammatory cytokines in macrophages. Unexpectedly, the mRNA of IL-1β, IL-6, and TNF-α did not alter in CNS-infiltrating macrophages of ghrelin-treated mice compared with the control mice (Fig. 7*A*). We next examined the expression of these cytokines in other cell types also known as a source of inflammatory cytokines and found reduced expression of these cytokines in microglia (Fig. 7*B*). Additionally, the expression of inflammatory cytokines was decreased in CNS-infiltrating T cells (Fig. 7*C*). Hence, these results suggest that microglia might play a crucial role in ghrelin-mediated inhibition of EAE.

Ghrelin inhibits the proinflammatory cytokine production of LPS-stimulated microglia

We next examined the effect of ghrelin on microglia. To test whether ghrelin directly affects microglia, we isolated mononuclear cells from the brains of untreated mice. In untreated non-EAE mice, most (~77%) of the brain mononuclear cells were $CD11b^+$ cells, and the majority of $CD11b^+$ cells (~95%) were considered as $CD45^{low}$ microglia cells. Among these mononuclear cells, $CD19^+$ B cells were <0.1% and $CD3^+CD45^+$ T cells were 1–1.5%. We cultured the isolated mononuclear cells in the presence of ghrelin overnight and stimulated them with LPS in different doses for 5 h. The TNF-α levels in the culture supernatant were measured by using ELISA. In the presence of ghrelin, the TNF-α levels were significantly reduced (Fig. 8). These results suggest that ghrelin directly affects microglia by reducing the production of inflammatory cytokines.

Discussion

Starvation is known to have immunosuppressive effects (24–26). Although little was known about the mechanistic link between starvation and immunity, recent studies have shed light on the immunomodulatory potency of a range of feeding regulatory hormones such as leptin and NPY. For example, serum leptin is decreased after acute starvation in parallel with immunosuppression or Th2 bias, whereas exogenous leptin would correct the altered Th1/Th2 balance toward Th1 (27, 28). In contrast, NPY is increased after starvation. Exogenous NPY would shift the Th1/Th2 balance toward Th2 and can ameliorate the severity of EAE (29). Interestingly, both peptide hormones are linked to ghrelin in an endocrine feedback system (30). Ghrelin itself is increased after

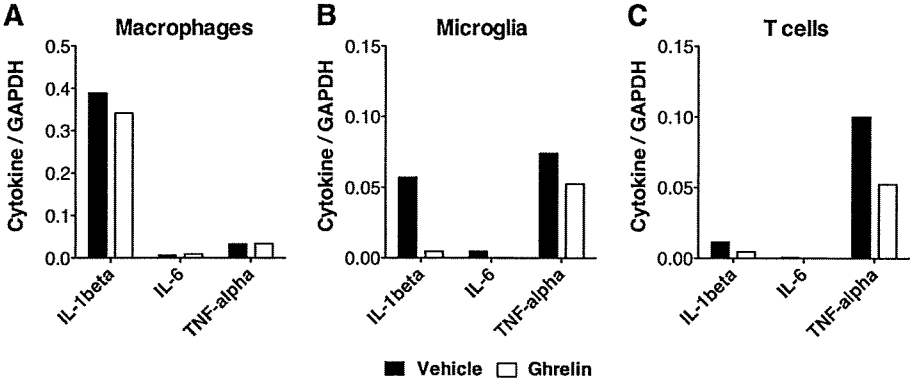

FIGURE 7. Effect of ghrelin on proinflammatory cytokine mRNA expression in infiltrating cells and microglia. Total mRNA was extracted from (*A*) macrophages, (*B*) microglia, and (*C*) T cells obtained on day 20 postimmunization from the spinal cords of MOG_{35-55}-immunized mice treated with ghrelin or saline. The IL-1β, IL-6, and TNF-α mRNA expression levels were measured by real-time PCR. Data are presented as relative amount of transcript normalized to the housekeeping gene GAPDH.

starvation, and it can potently stimulate the release of NPY in the CNS (12). Moreover, ghrelin shows antagonistic effects against leptin (31). Although the available data on the action of ghrelin on leptin or NPY may not be extrapolated to speculate about its role in the immune system, we decided to explore whether ghrelin may exhibit beneficial effects in the modulation of EAE. Furthermore, ghrelin was reported to have protective effects on endotoxic shock in rats (32). Additionally, the wide range of GHS-R expression within the immune cells strongly suggested the immunomodulatory potential of ghrelin (6). Considering its endocrine interactions, ghrelin becomes an interesting candidate for the in vivo modulation of EAE.

To evaluate the effects of ghrelin on the immune system in vivo, we used the representative EAE model induced with MOG_{35-55} in B6 mice. Subcutaneous injections of ghrelin significantly suppressed EAE severity, especially after the peak of disease, while the EAE onset occurred almost similarly in both ghrelin- and sham-treated mice. Priming phase treatment (days 1–10) as well as effector phase treatment (days 11–20) also showed disease-suppressing effects, suggesting a modulatory role of ghrelin during all phases of disease. The unacylated ghrelin form, des-acyl ghrelin, failed to suppress EAE, demonstrating that the disease suppression was mediated by the GHS-R.

The histological findings at day 17 were similar in all animals regardless of the applied treatment. The inflammatory cell infiltration and demyelination occurred in both groups, suggesting a ghrelin effect independent of cell trafficking at the peak of disease. Moreover, we found by FACS analysis that the number of mononuclear cells isolated from the spinal cord and their composition did not significantly alter among ghrelin- and sham-treated mice at the same time point. Our data showed no statistically significant changes in the examined cell subsets, which supported the histological findings of unaffected immune cell traffic to the CNS. This discrepancy between analogous inflammatory status in the spinal cord on the one hand and less severe disease on the other hand in ghrelin-treated mice was remarkable, suggesting cytokine regulation as the possible mechanism of EAE suppression.

Leptin and NPY both influence the Th1/Th2 balance in opposing directions (27–29). Since ghrelin is the most potent NPY-releasing hormone and NPY suppresses EAE by a Th2 bias (29), we examined whether ghrelin affects the Th1/Th2 balance similar to NPY and if its potential mechanism of EAE suppression is primarily mediated on immune cells or secondarily through NPY release. To investigate the effect of ghrelin on the cytokine balance, we measured the cytokine responses of MOG_{35-55}-primed T cells from mice treated with ghrelin or saline. The evaluated IFN-γ, IL-17, and IL-4 levels as well as the proliferative response did not significantly alter between ghrelin- and sham-treated mice. Underlying these observations, we conclude that the suppression of EAE mediated by ghrelin does not affect the T cell-derived cytokine balance. To further address whether ghrelin acts via the NPY pathway, we determined the encephalitogenic potential of $CD4^+$ T cells from ghrelin-treated mice to cause passive EAE in syngeneic recipients. We treated donor animals with ghrelin or saline for 10 days after priming with MOG_{35-55}, and lymphoid cells from the mice were stimulated with MOG_{35-55}. Three days later, $CD4^+$ T cell blasts were isolated and transferred to naive mice. The $CD4^+$ T cells from ghrelin-treated mice did not differ from those from saline-treated mice in the ability to mediate passive EAE, indicating that ghrelin does not primarily affect induction of encephalitogenic $CD4^+$ T cells in vivo. While NPY attenuates EAE by a Th2 bias of encephalitogenic $CD4^+$ T cells (29), our findings likely suggest that ghrelin interacts independently of NPY in the amelioration of EAE.

To further clarify the mechanism of ghrelin-mediated EAE suppression, we examined the mRNA levels of several cytokines of ghrelin- and sham-treated mice at the peak of disease. Our data demonstrate significantly reduced levels of the proinflammatory cytokines TNF-α, IL-1β, and IL-6 in the spinal cord and lower levels of TNF-α in the spleen of ghrelin-treated mice. In contrast, the level of TGF-β showed a trend for slight elevation in the spinal cord. The importance of TNF-α for initiating and sustaining inflammation is well described, as well as its essential role in the development of acute EAE (33, 34). The proinflammatory role of IL-1β and IL-6 in the immunopathology of EAE is also generally accepted (35–38). Thus, the inhibition of TNF-α, IL-1β, and IL-6 must be considered as an important mechanism in the ghrelin-mediated EAE suppression.

Given the selective down-modulation of the proinflammatory cytokines, we suspected that monocytes could be potential target cells in the ghrelin-mediated EAE suppression. However, the analysis of infiltrating cells and residential microglia revealed that the suppression of proinflammatory cytokines was prominently led by microglia. A decreased expression of these cytokines was also observed in infiltrating T cells. Considering that the transfer of T cells obtained from ghrelin-treated mice induced a similar disease course compared with control mice, the reduction of proinflammatory cytokines in microglia might be important in the ghrelin-mediated suppression of EAE.

In conclusion, the present study demonstrates for the first time to our knowledge that the gastric hormone ghrelin suppresses actively induced EAE by inhibiting production of the proinflammatory cytokines TNF-α, IL-1β, and IL-6 with microglia as the main target cells. These findings support an antiinflammatory property of ghrelin, shedding light on its role in immune-endocrine interactions. Consequently, we speculate that ghrelin may serve as an antiinflammatory drug to control human CNS pathology involving the production of proinflammatory cytokines.

Disclosures

The authors have no financial conflicts of interest.

References

1. Deghenghi, R., M. M. Cananzi, A. Torsello, C. Battisti, E. E. Muller, and V. Locatelli. 1994. GH-releasing activity of Hexarelin, a new growth hormone releasing peptide, in infant and adult rats. *Life Sci.* 54: 1321–1328.
2. Howard, A. D., S. D. Feighner, D. F. Cully, J. P. Arena, P. A. Liberator, C. I. Rosenblum, M. Hamelin, D. L. Hreniuk, O. C. Palyha, J. Anderson, et al. 1996. A receptor in pituitary and hypothalamus that functions in growth hormone release. *Science* 273: 974–977.
3. Smith, R. G., K. Cheng, W. R. Schoen, S. S. Pong, G. Hickey, T. Jacks, B. Butler, W. W. Chan, L. Y. Chaung, F. Judith, et al. 1993. A nonpeptidyl growth hormone secretagogue. *Science* 260: 1640–1643.
4. Kojima, M., H. Hosoda, Y. Date, M. Nakazato, H. Matsuo, and K. Kangawa. 1999. Ghrelin is a growth-hormone-releasing acylated peptide from stomach. *Nature* 402: 656–660.
5. Date, Y., M. Kojima, H. Hosoda, A. Sawaguchi, M. S. Mondal, T. Suganuma, S. Matsukura, K. Kangawa, and M. Nakazato. 2000. Ghrelin, a novel growth hormone-releasing acylated peptide, is synthesized in a distinct endocrine cell type in the gastrointestinal tracts of rats and humans. *Endocrinology* 141: 4255–4261.
6. Hattori, N., T. Saito, T. Yagyu, B. H. Jiang, K. Kitagawa, and C. Inagaki. 2001. GH, GH receptor, GH secretagogue receptor, and ghrelin expression in human T cells, B cells, and neutrophils. *J. Clin. Endocrinol. Metab.* 86: 4284–4291.
7. Hosoda, H., M. Kojima, H. Matsuo, and K. Kangawa. 2000. Ghrelin and des-acyl ghrelin: two major forms of rat ghrelin peptide in gastrointestinal tissue. *Biochem. Biophys. Res. Commun.* 279: 909–913.
8. Nakazato, M., N. Murakami, Y. Date, M. Kojima, H. Matsuo, K. Kangawa, and S. Matsukura. 2001. A role for ghrelin in the central regulation of feeding. *Nature* 409: 194–198.
9. Tschop, M., D. L. Smiley, and M. L. Heiman. 2000. Ghrelin induces adiposity in rodents. *Nature* 407: 908–913.
10. Muccioli, G., M. Tschop, M. Papotti, R. Deghenghi, M. Heiman, and E. Ghigo. 2002. Neuroendocrine and peripheral activities of ghrelin: implications in metabolism and obesity. *Eur. J. Pharmacol.* 440: 235–254.

11. Nagaya, N., T. Itoh, S. Murakami, H. Oya, M. Uematsu, K. Miyatake, and K. Kangawa. 2005. Treatment of cachexia with ghrelin in patients with COPD. *Chest* 128: 1187–1193.
12. Cowley, M. A., R. G. Smith, S. Diano, M. Tschop, N. Pronchuk, K. L. Grove, C. J. Strasburger, M. Bidlingmaier, M. Esterman, M. L. Heiman, et al. 2003. The distribution and mechanism of action of ghrelin in the CNS demonstrates a novel hypothalamic circuit regulating energy homeostasis. *Neuron* 37: 649–661.
13. Shintani, M., Y. Ogawa, K. Ebihara, M. Aizawa-Abe, F. Miyanaga, K. Takaya, T. Hayashi, G. Inoue, K. Hosoda, M. Kojima, et al. 2001. Ghrelin, an endogenous growth hormone secretagogue, is a novel orexigenic peptide that antagonizes leptin action through the activation of hypothalamic neuropeptide Y/Y1 receptor pathway. *Diabetes* 50: 227–232.
14. Dixit, V. D., E. M. Schaffer, R. S. Pyle, G. D. Collins, S. K. Sakthivel, R. Palaniappan, J. W. Lillard, Jr., and D. D. Taub. 2004. Ghrelin inhibits leptin- and activation-induced proinflammatory cytokine expression by human monocytes and T cells. *J. Clin. Invest.* 114: 57–66.
15. Wassem, T., M. Duxbury, H. Ito, S. W. Ashley, and M. K. Robinson. 2008. Exogeneous ghrelin modulates release of pro- and anti-inflammatory cytokines in LPS-stimulated macrophages through distinct signaling pathways. *Surgery* 143: 334–342.
16. Chorny, A., P. Anderson, E. Gonzalez-Rey, and M. Delgado. 2008. Ghrelin protects against experimental sepsis by inhibiting high-mobility group box 1 release and by killing bacteria. *J. Immunol.* 180: 8369–8377.
17. Gonzalez-rey, E., A. Chorny, and M. Delgado. 2006. Therapeutic action of ghrelin in a mouse model of colitis. *Gastroenterology* 130: 1707–1720.
18. Granado, M., T., Priego, A. I., Martin, A., Villanua, and A. Lopez-Caldron. 2005. Anti-inflammatory effect of the ghrelin agonist growth hormone-releasing peptide-2 (GHRP-2) in arthritic rats. *Am. J. Physiol.* 288: E486–E492.
19. Li, W. G., D. Gavrila, X. Liu, L. Wang, S. Gunnlaugsson, L. L. Stoll, M. L. McCormick, C. D. Sigmund, C. Tang, and N. L. Weintraub. 2004. Ghrelin inhibits proinflammatory responses and nuclear factor-κB activation in human endothelial cells. *Circulation* 109: 2221–2226.
20. Wu, R., W. Dong, X. Cui, M. Zhou, H. H. Simms, T. S. Ravikumar, and P. Wang. 2007. Ghrelin down-regulates proinflammatory cytokines in sepsis through activation of the vagus nerve. *Ann. Surg.* 245: 480–486.
21. Mendel, I., N. Kerlero de Rosbo, and A. Ben-Nun. 1995. A myelin oligodendrocyte glycoprotein peptide induces typical chronic experimental autoimmune encephalomyelitis in H-2b mice: fine specificity and T cell receptor Vβ expression of encephalitogenic T cells. *Eur. J. Immunol.* 25: 1951–1959.
22. Zhang, B., T. Yamamura, T. Kondo, M. Fujiwara, and T. Tabira. 1997. Regulation of experimental autoimmune encephalomyelitis by natural killer (NK) cells. *J. Exp. Med.* 186: 1677–1687.
23. Miyamoto, K., S. Miyake, M. Mizuno, N. Oka, S. Kusunoki, and T. Yamamura. 2006. Selective COX-2 inhibitor celecoxib prevents experimental autoimmune encephalomyelitis through COX-2-independent pathway. *Brain* 129: 1984–1992.
24. Chan, J. L., G. Matarese, G. K. Shetty, P. Raciti, I. Kelesidis, D. Aufiero, V. De Rosa, F. Perna, S. Fontana, and C. S. Mantzoros. 2006. Differential regulation of metabolic, neuroendocrine, and immune function by leptin in humans. *Proc. Natl. Acad. Sci. USA* 103: 8481–8486.
25. Kuchroo, V. K., and L. B. Nicholson. 2003. Immunology: fast and feel good? *Nature* 422: 27–28.
26. Wing, E. J., D. M. Magee, and L. K. Barczynski. 1988. Acute starvation in mice reduces the number of T cells and suppresses the development of T-cell-mediated immunity. *Immunology* 63: 677–682.
27. Lord, G. M., G. Matarese, J. K. Howard, R. J. Baker, S. R. Bloom, and R. I. Lechler. 1998. Leptin modulates the T-cell immune response and reverses starvation-induced immunosuppression. *Nature* 394: 897–901.
28. Sanna, V., A. Di Giacomo, A. La Cava, R. I. Lechler, S. Fontana, S. Zappacosta, and G. Matarese. 2003. Leptin surge precedes onset of autoimmune encephalomyelitis and correlates with development of pathogenic T cell responses. *J. Clin. Invest.* 111: 241–250.
29. Bedoui, S., S. Miyake, Y. Lin, K. Miyamoto, S. Oki, N. Kawamura, A. Beck-Sickinger, S. von Horsten, and T. Yamamura. 2003. Neuropeptide Y (NPY) suppresses experimental autoimmune encephalomyelitis: NPY1 receptor-specific inhibition of autoreactive Th1 responses in vivo. *J. Immunol.* 171: 3451–3458.
30. Kalra, S. P., and P. S. Kalra. 2003. Neuropeptide Y: a physiological orexigen modulated by the feedback action of ghrelin and leptin. *Endocrine* 22: 49–56.
31. Kalra, S. P., N. Ueno, and P. S. Kalra. 2005. Stimulation of appetite by ghrelin is regulated by leptin restraint: peripheral and central sites of action. *J. Nutr.* 135: 1331–1335.
32. Chang, L., J. Zhao, J. Yang, Z. Zhang, J. Du, and C. Tang. 2003. Therapeutic effects of ghrelin on endotoxic shock in rats. *Eur. J. Pharmacol.* 473: 171–176.
33. Glabinski, A. R., B. Bielecki, J. A. Kawczak, V. K. Tuohy, K. Selmaj, and R. M. Ransohoff. 2004. Treatment with soluble tumor necrosis factor receptor (sTNFR):Fc/p80 fusion protein ameliorates relapsing-remitting experimental autoimmune encephalomyelitis and decreases chemokine expression. *Autoimmunity* 37: 465–471.
34. Xanthoulea, S., M. Pasparakis, S. Kousteni, C. Brakebusch, D. Wallach, J. Bauer, H. Lassmann, and G. Kollias. 2004. Tumor necrosis factor (TNF) receptor shedding controls thresholds of innate immune activation that balance opposing TNF functions in infectious and inflammatory diseases. *J. Exp. Med.* 200: 367–376.
35. Furlan, R., A. Bergami, E. Brambilla, E. Butti, M. G. De Simoni, M. Campagnoli, P. Marconi, G. Comi, and G. Martino. 2007. HSV-1-mediated IL-1 receptor antagonist gene therapy ameliorates MOG_{35-55}-induced experimental autoimmune encephalomyelitis in C57BL/6 mice. *Gene Ther.* 14: 93–98.
36. Okuda, Y., S. Sakoda, H. Fujimura, Y. Saeki, T. Kishimoto, and T. Yanagihara. 1999. IL-6 plays a crucial role in the induction phase of myelin oligodendrocyte glucoprotein 35–55 induced experimental autoimmune encephalomyelitis. *J. Neuroimmunol.* 101: 188–196.
37. Okuda, Y., S. Sakoda, Y. Saeki, T. Kishimoto, and T. Yanagihara. 2000. Enhancement of Th2 response in IL-6-deficient mice immunized with myelin oligodendrocyte glycoprotein. *J. Neuroimmunol.* 105: 120–123.
38. Sutton, C., C. Brereton, B. Keogh, K. H. Mills, and E. C. Lavelle. 2006. A crucial role for interleukin (IL)-1 in the induction of IL-17-producing T cells that mediate autoimmune encephalomyelitis. *J. Exp. Med.* 203: 1685–1691.

Changes in pulmonary blood flow distribution in monocrotaline compared with hypoxia-induced models of pulmonary hypertension: assessed using synchrotron radiation

Daryl O. Schwenke[a], James T. Pearson[b], Akito Shimochi[c], Kenji Kangawa[d], Hirotsugu Tsuchimochi[e], Keiji Umetani[f], Mikiyasu Shirai[g,*] and Patricia A. Cragg[a,*]

Background We have previously described anatomical changes in pulmonary blood flow distribution in chronic hypoxic rats, associated with pulmonary arterial hypertension (PAH).

Method In this study, we utilized synchrotron radiation microangiography to compare these changes in pulmonary blood flow with a PAH-model induced with monocrotaline (MCT), as the etiology for these two models of PAH is different. Three weeks after a subcutaneous injection of MCT (60 mg/kg) or vehicle (control), Sprague–Dawley rats were anesthetized, and microangiography was performed on the left lung to assess branching distribution of pulmonary blood flow and changes in vessel diameter during acute (8% O_2 for 4 min) hypoxic pulmonary vasoconstriction – before and after sympathetic β-adrenoceptor blockade (propranolol, 2 mg/kg, intravenous). Comparisons were made with chronic hypoxic rats using data previously published.

Results We observed that adverse changes in pulmonary blood flow were comparable for both chronic hypoxia and MCT models of PAH. Specifically, the number of opaque third and fourth generation vessels was significantly and equally fewer than that of control rats. The acute hypoxic pulmonary vasoconstriction was not altered in the hypertensive lung, though sympathetic modulation of pulmonary vasoreactivity was enhanced by chronic hypoxia, but not MCT.

Conclusion In summary, we have demonstrated comparable adverse changes in pulmonary blood flow for chronic hypoxia and MCT models of PAH. In contrast, modulation of the hypoxic pulmonary vasoconstriction differs between the two PAH models, likely due to the impact that different pathological pathways have on the physiology of the whole organism. Such differences between models of PAH should be considered in future studies. *J Hypertens* 27:1410–1419 © 2009 Wolters Kluwer Health | Lippincott Williams & Wilkins.

Journal of Hypertension 2009, 27:1410–1419

Keywords: hypoxia, monocrotaline, pulmonary microvessels, rat, synchrotron radiation microangiography

Abbreviations: HPV, hypoxic pulmonary vasoconstriction; HR, heart rate; MABP, mean arterial pressure; MCT, monocrotaline; O_2, oxygen; PAH, pulmonary arterial hypertension; PAP, pulmonary arterial pressure; RVP, right ventricular pressure

[a]Department of Physiology, University of Otago, Dunedin, New Zealand, [b]Department of Physiology and Monash Centre for Synchrotron Science, Monash University, Melbourne, Australia, [c]Department of Etiology and Pathogenesis, National Cardiovascular Center Research Institute, [d]Department of Biochemistry, [e]Department of Cardiac Physiology, National Cardiovascular Center Research Institute, Suita, Osaka, [f]Japan Synchrotron Radiation Research Institute, Hyogo and [g]Faculty of Health Sciences, Hiroshima International University, Hiroshima, Japan

Correspondence to Dr Daryl O. Schwenke, Department of Physiology, University of Otago, PO Box 56, Dunedin, New Zealand
Tel: +81 64 3 479 7330; fax: +81 64 3 479 7323;
e-mail: daryl.schwenke@stonebow.otago.ac.nz

Received 3 November 2008 Revised 8 February 2009
Accepted 26 February 2009

Introduction

Pulmonary arterial hypertension (PAH) is a common adverse complication associated with several cardiopulmonary disorders and has a bleak long-term prognosis. PAH is characterized by a sustained increase in pulmonary arterial pressure (PAP) that increases the workload of the heart and is, therefore, closely associated with heart failure and increased mortality [1]. Although significant advances in the treatment of PAH have been made in recent decades, the underlying mechanisms governing the pathogenesis of PAH remain to be fully elucidated. Our understanding may be confounded because the etiology for different models of PAH, such as monocrotaline (MCT) and chronic hypoxia, may not be similar [2–4]. Indeed, the literature seems to suggest that both the cellular signal pathways that are involved in the pathogenesis of these forms of PAH, and the resultant morphological changes in the pulmonary vasculature, may differ between chronic hypoxia and MCT [3–6].

Whether these cellular and morphological differences between MCT and chronic hypoxia ultimately culminate in differing patterns of pulmonary blood flow distribution is not currently known. Yet, it is these changes in blood

*M.S. and P.A.C. contributed equally to the writing of this article.

0263-6352 © 2009 Wolters Kluwer Health | Lippincott Williams & Wilkins DOI:10.1097/HJH.0b013e32832af6a1

flow distribution, regardless of cause, which are responsible for the adverse increase in PAP. Importantly, any discrepancies in the pathological alterations of pulmonary blood flow between chronic hypoxia and MCT may impact on the type, and effectiveness, of potential therapeutic interventions [3].

The ability to compare pathological changes in pulmonary blood flow between different PAH models has, up until recently, been restricted due to methodological limitations for assessing the pulmonary microcirculation, especially within the natural physiological milieu of a closed-chest animal model. In a recent study, we utilized synchrotron radiation microangiography (i.e. radiograph) for assessing in detail the anatomical and functional changes of the pulmonary circulation associated with chronic hypoxia-induced PAH in a closed-chest rat model [7].

In this study, we aimed to assess the changes in pulmonary blood flow distribution following MCT-induced PAH and compare it with those results previously obtained from chronic hypoxic rats. We utilized synchrotron radiation microangiography, which has enhanced sensitivity to contrast material and superior visualization of pulmonary vessels compared with more conventional angiography methods. The results from this study will help to ascertain whether the nature of change in pulmonary blood flow distribution in two distinctly different models of PAH is etiology dependent.

Materials and methods

Animals

Experiments were conducted on 14 male Sprague–Dawley rats (9 weeks old; body weight $\sim$200–280 g). Three weeks prior to experimentation, rats received a subcutaneous injection of either MCT (0.5 ml, 60 mg/kg in 0.2 N HCl; Sigma, St Louis, Missouri, USA; $n=7$) or vehicle alone (0.5 ml; $n=7$). All rats were on a 12 h light/dark cycle at 25 $\pm$ 1°C and were provided with food and water *ad libitum*. All experiments were conducted at the Japan Synchrotron Radiation Research Institute, Hyogo, Japan. Experiments were approved by the local Animal Ethics Committee and conducted in accordance with the guidelines of the Physiological Society of Japan.

Anesthesia and surgical preparation

Three weeks after MCT/vehicle injection, rats were anesthetized with pentobarbital sodium [60 mg/kg, intraperitoneally (i.p.)]. Supplementary doses of anesthetic were periodically administered ($\sim$15 mg/kg per h i.p.). Throughout the experimental protocol, body temperature was maintained at 37°C using a rectal thermistor coupled with a thermostatically controlled heating pad.

The trachea was cannulated and the lungs ventilated with a rodent ventilator (SN-480-7; Shinano, Tokyo, Japan). The inspirate gas was enriched with O_2 ($\sim$50% O_2), and the ventilator settings were adjusted (tidal volume $\sim$3.5 ml; freq. $\sim$70/min). A femoral artery and vein were cannulated for measurement of systemic arterial blood pressure (ABP) and drug administration, respectively. A 20-gauge BD Angiocath catheter (Becton Dickinson, Inc., Sandy, Utah, USA), with the tip at a 30-degree angle, was inserted into the jugular vein and advanced into the right ventricle for administering contrast agent as well as intermittently measuring right ventricular pressure (RVP).

The rat was securely fastened supine to a clear Perspex surgical plate, which had a single window opening directly beneath the thorax area. The surgical plate was then fixed in a vertical position in front of the beam pathway, so that the synchrotron beam would pass perpendicular to the sagittal plane from anterior to posterior through the rat thorax and ultimately to a SATICON X-ray camera described below.

Microangiographic system

The pulmonary circulation was visualized using synchrotron radiation microangiography at the SPring-8 BL28B2 beam line facility, Hyogo, Japan (Fig. 1). The use of synchrotron radiation for visualizing the pulmonary microcirculation in the closed-chest rat has previously been described in detail [7,8].

In brief, synchrotron radiation has a broad and continuous spectrum from the infrared to the X-ray regions. A single crystal monochromator was used to select a single energy of synchrotron radiation, producing X-rays of a very narrow energy bandwidth for imaging. This synchrotron radiation system comprised a monochromatic 33.2-keV X-ray source, just above the iodine K-edge energy for maximal contrast.

X-rays transmitted through a patient are detected by an X-ray detector (Hitachi Denshi Techno-System, Ltd., Tokyo, Japan) incorporating a SATICON X-ray pickup tube (Hamamatsu Photonics K.K., Shizuoka, Japan). The biomedical imaging SATICON X-ray camera has a resolution of 1050 scanning lines and can record images at a maximum speed of 30 frames/s for up to 30 s. The shutter open-time used in this study was 2.6–3.0 ms per frame. The detector features a 9.5-μm equivalent pixel size that captures a 9.5 $\times$ 9.5 mm input field size. High-resolution images were stored in a digital frame memory system with 1024 $\times$ 1024 pixel format and 10-bit resolution.

Experimental protocol

The rat was positioned in front of the beam so that the upper segment of the left lobe was positioned in front of the SATICON X-ray camera in alignment with the 9.5 $\times$ 9.5 mm imaging field (i.e. between the second and third rib; Fig. 1). Preliminary experiments identified that

Fig. 1

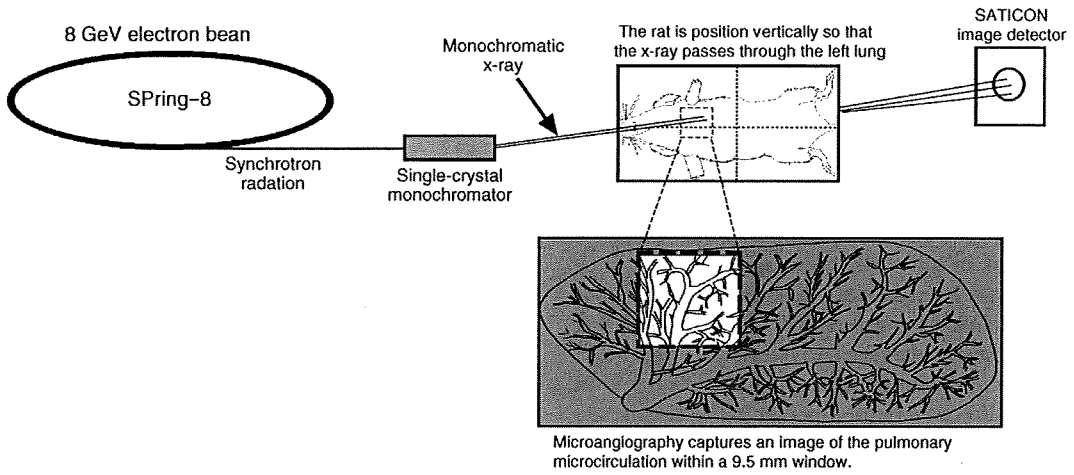

A simplified schematic diagram showing the experimental set-up for pulmonary microangiography in a closed-chest rat model using monochromatic synchrotron radiation and the region of the left lung used for capturing angiographic images representative of the pulmonary microcirculation.

this segment of the lung best represented the pulmonary circulation as a whole in terms of anatomical layout and vascular responsiveness. Subsequently, baseline heart rate (HR), RVP and ABP data were collected. Immediately prior to vessel imaging, the three-way stopcock on the right ventricle catheter was opened to a clinical autoinjector (Nemoto Kyorindo, Tokyo, Japan), which was used to inject a single bolus of contrast agent (Iomeron 350; Eisai Co. Ltd, Tokyo, Japan) at high speed (0.4 ml at 0.4 ml/s). For each 2-s period of scanning (a single exposure sequence), 100 frames were recorded. Rats were given at least 10 min to recover from each bolus injection of contrast agent. Regular inspection between contrast injections confirmed that the pulmonary vasculature was clear of agent within this period of time.

Following baseline imaging, rats were exposed to acute hypoxia (8% O_2 in N_2) for 4 min. During acute hypoxia, ABP, HR and RVP data were continuously recorded until the third minute, after which recording of RVP was stopped, and the catheter was switched from the pressure transducer to the clinical injector for imaging. Lung microangiography was performed on the hypoxic lung after the fourth minute of hypoxia.

Upon recovery from the acute hypoxic test, rats were administered the β-receptor blocker, propranolol [2 mg/kg, intravenous (i.v.)]. After waiting 10–15 min for all cardiovascular variables to stabilize, pulmonary microangiography was repeated before and after acute hypoxia.

Data acquisition and analysis

The RVP and ABP signals were detected using separate Deltran pressure transducers (Utah Medical Products, Inc., Salt Lake City, Utah, USA), the signals were relayed to Powerlab bridge amplifiers (ML117, AD Instruments Pty Ltd, Japan, Inc., Izumi, Japan), and then continuously sampled at 500 Hz with an eight-channel MacLab/8s interface hardware system (AD Instruments), and recorded on a Macintosh Power Book G4 using Chart (v. 5.0.1, AD Instruments). HR was derived from the arterial systolic peaks.

From the 2-s period of image collection, one frame per scan (one frame sequence = 100 frames) was selected for image enhancement and analysis. Furthermore, only those frames recorded at, or near, end systole were used for assessing and comparing pulmonary vessel diameter between baseline and hypoxic conditions.

All imaged vessel branches were counted. Where possible, the widths of two to four vessels of each branching generation (second to fourth generation) were measured to ensure a wide variety of vessel sizes were selected from each frame. Vessels were categorized according to internal diameter lengths of 100–200 μm, 200–300 μm, 300–500 μm and more than 500 μm. Accordingly, the internal diameter of 67 vessels, comprising the four branching generations, was measured in seven control rats. Similarly, 64 vessels were measured in seven MCT-rats. The internal diameter of individual vessels was measured before and after acute hypoxia, with and without β-receptor blockade (i.e. propranolol treatment).

Image analysis

The computer-imaging program Image Pro-plus (ver. 4.1, Media Cybernetics, Bethesda, Maryland, USA) was used to enhance contrast and the clarity of angiogram images. To enhance images, a temporal subtraction operation was

performed for flat-field correction using summation results of 10 consecutive frames acquired before contrast-agent injection. The summation image taken before injection was subtracted from a single raw image taken after injection to eliminate the superimposed background structure.

Image Pro-plus was also used to evaluate the vessel internal diameter. A 50-μm thick tungsten filament, which had been placed directly across the corner of the detector's window, appeared in all recorded images and was subsequently used as a reference for calculating vessel diameter (μm). The line-profile function of Image Pro-Plus was used to measure changes in pixel intensity (brightness) along manually drawn segments spanning 10–40 pixels on either side in the direction perpendicular to the vessel (see [8]). The reliability for measuring vessel internal diameter is highly reproducible between independent observers based on regression analysis ($r^2 = 0.975$), with an average difference of 6 ± 3 μm (for 100–200 μm vessels) to 9 ± 4 μm (for 300–500 μm vessels) [7,8].

Statistical analysis

All statistical analyses were conducted using Statview (v5.01; SAS Institute, Cary, North Carolina, USA). All results are presented as means ± standard error of the mean (SEM). Two-way analysis of variation (ANOVA) (repeated measures) was used to test whether propranolol significantly altered the dynamic pulmonary vasoconstriction response to acute hypoxia. One-way ANOVA (factorial) was used to test for differences in vessel caliber during normoxia and acute hypoxia and baseline values for control rats (cont-rats) compared with MCT-treated rats and values for MCT-rats compared with chronic hypoxic rats. Where statistical significance was reached, post hoc analyses were incorporated using the paired or unpaired *t*-test with the Dunnet's correction for multiple comparisons. A P value of 0.05 or less was predetermined as the level of significance for all statistical analysis.

Results

Baseline

Baseline hemodynamic data are presented in Table 1. MCT-induced PAH, evident as systolic RVP, was approximately 70% higher than that of cont-rats ($P < 0.01$). Comparatively, the magnitude of PAH for MCT-rats was smaller than that observed in rats exposed to chronic hypoxia (chronic hypoxic rats) for 4 weeks [~120% increase in systolic right ventricular pressure (sRVP); see Table 1]. Both MCT and chronic hypoxia did not significantly alter mean ABP (MABP) or HR.

Using synchrotron radiation, we were able to clearly assess the adverse changes in the pulmonary circulation associated with MCT-induced PAH. Figure 2 shows typical microangiograms of the pulmonary circulation, from the main axial artery of the left lobe to the 4th generation of branching (within the 9.5 × 9.5 mm imaging window), of a cont-rat, a MCT-rat and, for comparative purposes, a chronic hypoxic rat (taken from [7]). Interestingly, the adverse anatomical changes in pulmonary blood flow distribution for MCT-rats were remarkably similar to that observed for chronic hypoxic rats.

Table 1 Systolic right ventricular pressure, mean arterial pressure and heart rate data of the anesthetized control rats (cont-rats; $n = 7$) and rats with PAH induced by monocrotaline (PAH-rats; $n = 7$), before and after propranolol administration (2 mg/kg, i.v.)

	sRVP (mmHg)	MABP (mmHg)	HR (b/min)
Physiological saline			
Cont-rats	25.2 ± 1.0	115 ± 6	403 ± 8
	(24.3 ± 1.0)	(103 ± 7)	(338 ± 13)
MCT-rats	42.8 ± 2.4†	108 ± 6	404 ± 13
CH rats	(53.1 ± 2.0†)	(118 ± 4)	(353 ± 13)
Propranolol			
Cont-rats	26.7 ± 1.4	111 ± 6	355 ± 16*
	(27.3 ± 1.4)	(105 ± 6)	(319 ± 4)
MCT-rats	43.0 ± 1.8†	93 ± 8	332 ± 9†,*
CH rats	(54.2 ± 1.7†)	(136 ± 3†,*)	(294 ± 5†,*)

Data presented in parentheses are from separate groups of cont ($n = 5$) and CH rats ($n = 5$) from [7]. Data are presented as mean ± SEM. CH, chronic hypoxic; HR, heart rate; MAP, mean arterial pressure; sRVP, systolic right ventricular pressure. † Significantly different from cont-rats ($P < 0.01$). * Significant difference between saline and propranolol ($P < 0.01$).

Vessel number

The total number of opaque vessel branches visible within each baseline image (i.e. 9.5 × 9.5 mm imaging window) was counted. As illustrated in Fig. 3a, pulmonary hypertension was associated with a decrease in the number of opaque third and fourth generation vessels, regardless of whether the etiology was induced by MCT (9 ± 1 and 20 ± 1 vessels, respectively) or chronic hypoxia (9 ± 1 and 16 ± 2 vessels, respectively), compared with cont-rats (12 ± 1 and 26 ± 2 vessels, respectively; $P < 0.05$). Interestingly, the number of fourth generation vessels was marginally fewer for chronic hypoxic rats (nonsignificant) compared with MCT-rats, possibly reflecting the higher PAP in chronic hypoxia-induced PAH. The number of first and second generation branches was not significantly altered by either MCT or chronic hypoxia (2 and 4–5, respectively).

Vessel size

Vessel internal diameter tended to decrease according to each generation of branching, as well as the distance away from the main axial artery towards the periphery (Fig. 3b). The internal diameter of the first generation branch was similar for cont-rats (556 ± 37) and MCT-rats (596 ± 29). Chronic hypoxia, however, significantly increased the internal diameter of the first generation branch (740 ± 53 μm) – possibly due to a more severe magnitude of PAH (i.e. the higher distending pressure) for chronic hypoxic rats, compared with MCT-rats. Vessel caliber was not significantly different between cont-rats, MCT-rats and chronic hypoxic rats for the second to fourth generation of branching (Fig. 3b).

Fig. 2

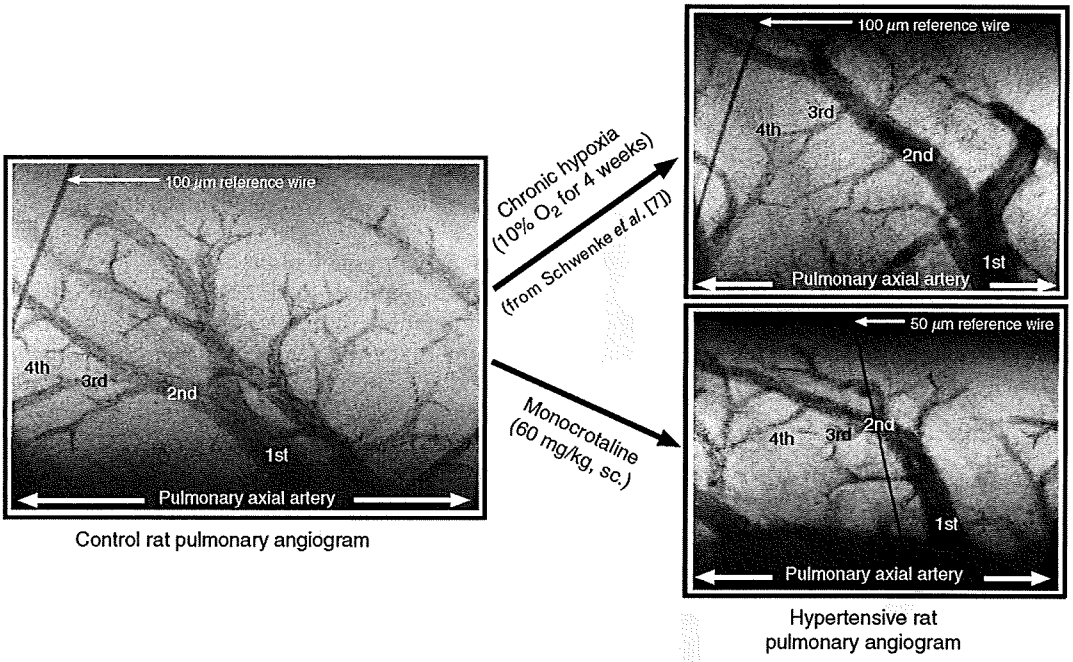

Typical microangiogram images showing the branching pattern of small pulmonary arteries in control rats (cont-rat; $n=7$) and rats with pulmonary arterial hypertension, which was induced with either monocrotaline (MCT-rat; $n=7$) or chronic hypoxia (chronic hypoxic rat; $n=5$; data taken from 8]). Pulmonary branches to the fourth generation from the left main axial artery were visible. MCT, monocrotaline.

Responses to acute hypoxia

Pulmonary vascular reactivity was assessed by exposing rats to acute hypoxia (8% O_2 for 4 min). Acute hypoxia caused a significant decrease in the internal diameter of all vessels smaller than 500 μm (cont-rats) or less than 300 μm (MCT-rats) (Fig. 4). In all rats, the magnitude of constriction tended to increase as vessel caliber decreased, with the greatest degree of vasoconstriction occurring in those vessels with a diameter between 100 and 300 μm. These vessels were generally of the third to fourth generation of branching. The magnitude of hypoxic pulmonary vasoconstriction (HPV) for all vessel sizes was similar for control rats and pulmonary hypertensive rats – regardless of whether PAH was induced by MCT or chronic hypoxia.

Similarly, the hemodynamic responses to acute hypoxia were not altered after the development of PAH (for both MCT and chronic hypoxia) (Fig. 5). Therefore, acute hypoxia consistently induced a significant increase in systolic RVP (21–27%; $P<0.01$), a decrease in MABP (40–45% decrease, $P<0.01$) but did not significantly change HR.

Responses to propranolol

Rats were administered the sympathetic β-receptor blocker, propranolol (2 mg/kg, i.v.). In both cont-rats and MCT-rats, propranolol did not significantly alter baseline pulmonary vessel caliber for any of the vessel size groups analyzed, also reflected in the lack of significant response of systolic RVP to propranolol (Table 1). Similar RVP responses were reported for chronic hypoxic rats [7]. In both cont-rats and MCT-rats, propranolol did not change MABP, but it did significantly reduce HR by approximately 16%. In chronic hypoxic rats, propranolol significantly increased MABP (15% increase) and caused a 17% decrease in HR ($P<0.01$).

In cont-rats, β-receptor blockade exacerbated the magnitude of acute hypoxic vasoconstriction in 200–300 μm-sized pulmonary vessels (Fig. 4), though statistical significance was not achieved as we have previously reported [7]. The systolic RVP, MABP and HR responses to acute hypoxia were unaltered following propranolol treatment (Fig. 5). MCT-induced PAH did not alter the vessel dynamic response (Fig. 4) or hemodynamic responses to acute hypoxia (Fig. 5). In comparison, we have previously shown that β-receptor blockade in chronic hypoxic rats significantly accentuates the systolic RVP response to acute hypoxia ($P<0.05$), reflecting extensive pulmonary vasoconstriction in 200–300 μm-sized vessels and, unlike that observed for cont-rats, even greater constriction in 100–200 μm-sized vessels (Fig. 4).

Fig. 3

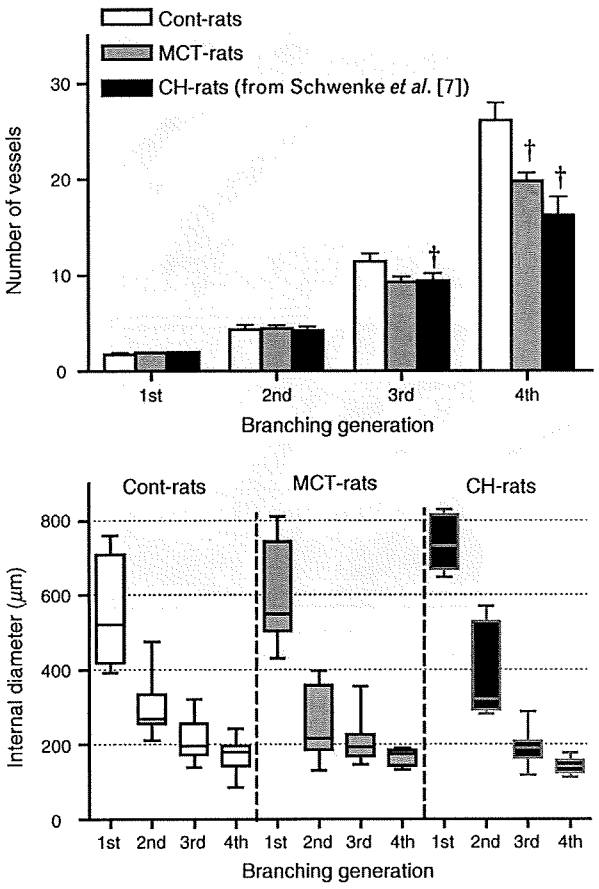

Changes in (a) the number of opaque vessels (mean ± SEM), (b) the range of vessel sizes (box and whisker graph) at each of the first four branching generations of the pulmonary circulation in control rats (cont-rats; $n = 7$), monocrotaline-treated rats (MCT-rats, $n = 7$) and chronic hypoxic rats (chronic hypoxic rats; $n = 5$). †Significantly different from cont-rats ($P < 0.05$). There was no significant difference between MCT-rats and chronic hypoxic rats. CH, chronic hypoxic; MCT, monocrotaline.

Evaluation of accuracy of measurement

Two techniques have previously been used for evaluating the accuracy of measurement [7,8]. In brief, first we estimated a margin of error for detecting the edge of a vessel by assessing pixel variability of a tungsten reference wire, with a known diameter of 100 μm and reported a margin of error of approximately 5 μm (range 97–103 μm). Second, we performed phantom measurements to assess the relationship between X-ray absorption and iodine concentration (for more detail, see [8]). The results show that measurements of approximately 100 μm in diameter can be made with the required precision for those vessels with an iodine concentration of 64 mg/μl or greater – a concentration considerably lower than that in this study.

Discussion

Using synchrotron radiation microangiography, we have effectively demonstrated comparable adverse anatomical changes in pulmonary blood flow distribution for both MCT and chronic hypoxia PAH models. Additionally, pulmonary vasoreactivity in response to acute hypoxia remains unchanged following the pathogenesis of PAH, though sympathetic modulation of pulmonary vasoreactivity is altered by chronic hypoxia but not MCT.

Pulmonary arterial hypertension

PAH is a common complication associated with numerous pulmonary disorders. Despite decades of research, the underlying cellular mechanisms governing the pathogenesis of PAH remain to be fully elucidated. This seemingly unending ambiguity may be, in part, due to the fact that the cause governing the pathogenesis of PAH differs depending on the type of pulmonary disorder. Regardless of cause, chronic PAH is associated with structural pulmonary vascular changes, right ventricular hypertrophy and ultimately heart failure [1].

MCT, a plant-derived pyrolizidine alkaloid, is often used in experimental animal models for simulating the vascular inflammatory symptoms commonly associated with several human interstitial lung diseases, which ultimately induce PAH. MCT initially causes selective pathological inflammation and damage to the pulmonary endothelium, which precedes vascular dysfunction and vascular remodeling [3]. Hypoxia, which is more commonly associated with chronic obstructive pulmonary disorders in humans, initially causes reversible pulmonary vasoconstriction (within minutes) that, when sustained over a long period of time, increases the shear stress within the pulmonary vasculature that then acts as the primary catalyst for endothelial cell injury–dysfunction [9] and vascular remodeling [10,11]. Structural changes in the pulmonary vasculature associated with chronic hypoxia are evident after 3 days. In comparison, the PAP response to MCT, which is primarily due to gradual morphological changes (no acute vasoconstriction), does not induce an increase in PAP until after approximately 21 days [4].

Vascular remodeling in the hypertensive lung is mediated through the impairment of various cellular signaling pathways within the smooth muscle and endothelium, some of which are common to both chronic hypoxia and MCT models and others that are specific for each model [12]. For example, the levels of endothelin-1 (ET-1), an endothelial-derived vasoconstrictor, are elevated in both the chronic hypoxia model [13–15] and the MCT model [16,17]. In contrast, the expression of endothelial nitric oxide synthase (eNOS) is reduced by MCT [3,17,18] but elevated in the chronic hypoxia model [12,13,19–21]. The consequence, however, is similar in that NO bioavailability or NO-dependent vasodilation or both are

Fig. 4

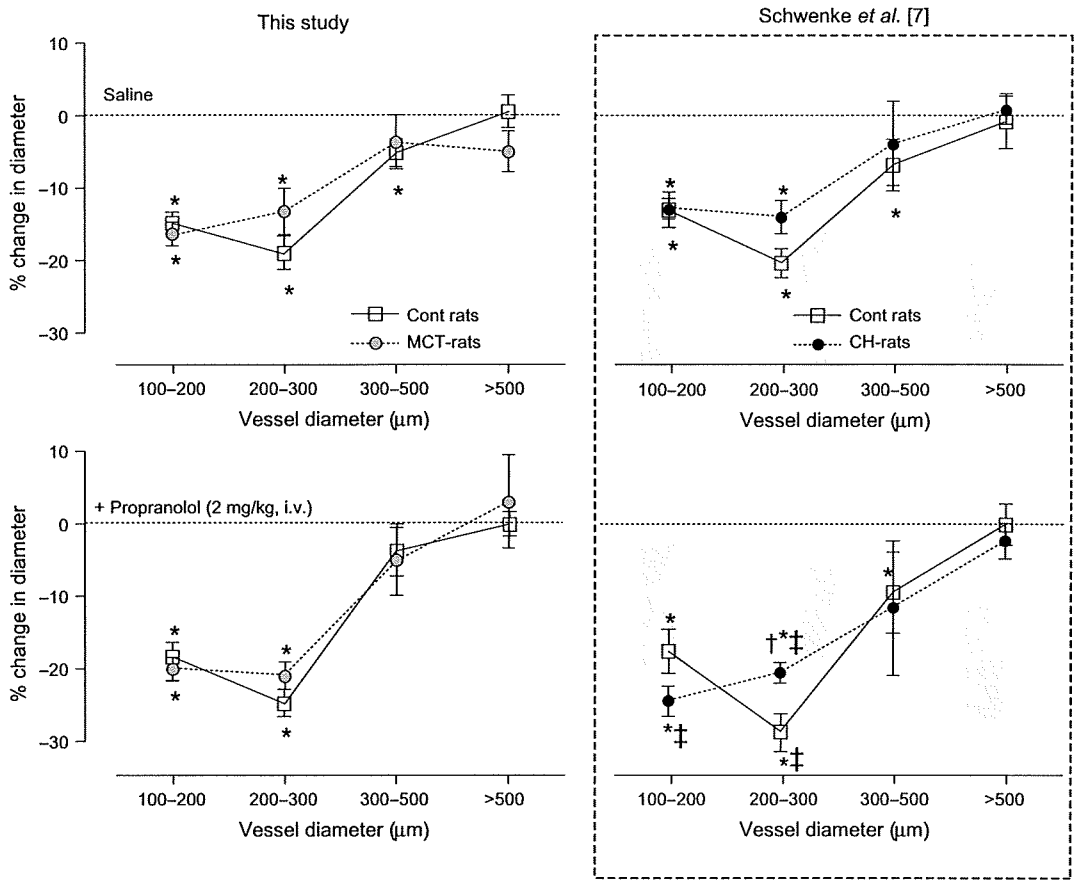

The relationship between vessel size and the magnitude of pulmonary vasoconstriction (% decrease in vessel diameter) in response to acute hypoxia (8% O_2 for 4 min) in control rats (cont-rats; $n=7$), monocrotaline-treated rats (MCT-rats, $n=7$) and chronic hypoxic rats (chronic hypoxic rats; $n=5$), before and after the i.v. administration of propranolol (2 mg/kg). *Significant vasoconstriction response to acute hypoxia ($P<0.05$). †Significant difference between cont-rats and chronic hypoxic rats ($P<0.05$). ‡Significant change in the magnitude of vasoconstriction following propranolol administration ($P<0.05$). MCT, monocrotaline.

blunted in both the chronic hypoxia model [22–25] and the MCT-model [3].

Synchrotron radiation

We have previously demonstrated the validity and accuracy of synchrotron radiation microangiography as a powerful tool for assessing pulmonary blood flow within a closed-chest rat model [7,8]. In this study, we utilized synchrotron radiation to effectively show for the first time that, regardless of the cause, the pathological changes in pulmonary blood flow distribution associated with PAH are comparable for both MCT and chronic hypoxia. Noticeably, we observed a reduction in the number of perfused arterioles of the third and fourth branching generations (internal diameter of 80–300 μm), which was similar for both MCT and chronic hypoxia. Furthermore, the degree of reduction was similar for both MCT-rat and chronic hypoxia-rat models (e.g. both chronic hypoxic and MCT-rats had ~25% fewer opaque vessels of the third generation compared with cont-rats). Importantly, it is this adverse change in pulmonary blood flow that is primarily responsible for the consequential increase in pulmonary vascular resistance and PAP.

We also observed that vessel size at each branching generation was similar for all three groups of rats, except that chronic hypoxic rats had a larger first generation branch compared with control and MCT-rats. This is likely due to a mechanical effect, that is, higher distending pressure in chronic hypoxic rats and not an elevated sympathetic tone, which is associated with chronic hypoxia (see below), as large conduit pulmonary vessels (>500 μm) are not influenced by changes in sympathetic tone. Rather, sympathetic modulation is primarily